Nano Research

ISSN 1998-0124 CN 11-5974/O4
https://doi.org/10.26599/NR.2026.94908723

Review Article

Curvature nanocarriers: From rational design to efficient applications

Naiwen Liu, Shuyi Pang, Xiaoxiao Zhang, Yuanduo Li, Hangkai Shi, Jiangping Lai(✉), Lei Wang(✉)
State Key Laboratory Base of Eco-Chemical Engineering, Ministry of Education, International Science and Technology Cooperation Base of Eco-chemical Engineering and Green Manufacturing, College of Chemistry and Molecular Engineering, Qingdao University of Science and Technology, Qingdao 266042, China

Nano Res., **Just Accepted Manuscript** • https://doi.org/10.26599/NR.2026.94908723
https://www.sciopen.com/journal/1998-0124 on Apr. 9, 2026

Just Accepted

DOI: 10.26599/NR.2026.94908723

Article type: review article

Curvature nanocarriers: From rational design to efficient applications

Naiwen Liu, Shuyi Pang, Xiaoxiao Zhang, Yuanduo Li, Hangkai Shi, Jiangping Lai, and Lei Wang**

State Key Laboratory Base of Eco-Chemical Engineering, Ministry of Education, International Science and Technology Cooperation Base of Eco-chemical Engineering and Green Manufacturing, College of Chemistry and Molecular Engineering, Qingdao University of Science and Technology, Qingdao 266042, China

Received: 18 January 2026; **Revised:** 23 March 2026; **Accepted:** 9 April 2026

Address correspondence to Jiangping Lai, jplai@qust.edu.cn; Lei Wang, inorchemwl@126.com

 **Cite this article:** *Nano Research*, 2026, 19, 94908723 https://doi.org/10.26599/NR.2026.94908723

Abstract: As a core geometric parameter of nanocarriers, curvature exerts crucial regulatory effects in diverse fields such as biomedicine, catalysis, and materials assembly. For nanocarriers with regular geometric morphologies, the absolute value of curvature is inversely proportional to their characteristic sizes (e.g., particle size, tube diameter), and the smaller the characteristic size, the more significant the curvature effect. This paper presents the first systematic review of the design and synthesis strategies of curvature-tailored nanocarriers, while also providing an in-depth discussion of their performance across multiple application scenarios. In terms of design and synthesis, this paper establishes a classification system encompassing positive curvature, negative curvature, and mixed curvature, introduces various curvature characterization techniques including electron microscopy, scattering methods, and atomic force microscopy, and summarizes precise curvature-control synthesis strategies such as the template method, self-assembly method, controlled buckling method, and etching method. In the aspect of application evaluation, curvature-tailored nanocarriers significantly enhance intracellular endocytosis efficiency and tumor tissue penetration capacity in drug delivery; in catalytic applications, they achieve improvements in catalyst performance by regulating electronic structures, reaction kinetics, and reaction mechanisms; in materials assembly, curvature serves as a structural modulation tool to promote the development of ordered assembled architectures. This paper provides systematic theoretical support and methodological guidance for the rational design and functionalized application of curvature-tailored nanocarriers, and further prospects their future development directions in intelligent design, multifunctional integration, and industrialization.

Keywords: curvature nanocarriers, medicine, catalysis, material assembly

1. Introduction

As a core geometric parameter of nanomaterials, curvature is increasingly emerging as a frontier and focal point of interdisciplinary research. At the nanoscale, curvature not only determines the physicochemical properties of material surfaces, but also plays a pivotal regulatory role in processes

such as biological interactions, catalysis, energy conversion, and matter assembly.[1-4] Quantitatively, the curvature of regular nanocarriers (e.g., spherical nanoparticles, carbon nanotubes) has a definite inverse correlation with their characteristic sizes, which is the fundamental basis for the precise regulation of curvature by adjusting the size of nanocarriers in synthesis. Notably, this correlation does not equate to a causal relationship, and the two parameters possess distinct physical connotations: size is a macroscopic dimensional parameter reflecting the overall volume or scale of nanocarriers, while curvature is a local topological parameter characterizing the surface bending degree and geometric distortion state. Critically, the same characteristic size can correspond to diverse curvature types (e.g., solid nanospheres and hollow nanobowls with identical diameters exhibit positive and negative curvature, respectively), and different sizes can be engineered to achieve consistent curvature via structural design, verifying that curvature is an independent design parameter decouplable from size. Compared with traditional isotropic spherical structures, nanocarriers with tailored curvature can precisely program their transport, catalytic, and assembly behaviors by modulating surface stress distribution, electron density of states, and interfacial interaction energy-a structural regulation mechanism essentially different from that of size or composition optimization, which mainly improve performance by altering specific surface area or chemical activity of active sites-thus demonstrating potential in fields like drug delivery, catalytic reactions, and superstructure construction.[5,6]

With the advancement of nanosynthesis technologies and characterization methods, curvature-related research has made progress in several sub-fields.[7,8] For example, reviews in the protein corona field often discuss the effects of surface curvature on biointerface interactions, and studies in single-atom catalysis frequently involve curvature/strain engineering for catalytic performance regulation, laying a foundation for the functional research of curvature. However, existing studies mostly regard curvature as an auxiliary feature scattered in various sub-fields, without realizing

cross-field systematic integration, and lack systematic research on curvature as an independent core design parameter. Scholars still lack a unified understanding of the cross-scale structure-activity relationship and generalized regulation strategies of curvature.[9-15] Nevertheless, this field still faces a series of challenges, including the standardized characterization of curvature parameters, the modeling of structure-activity relationships across scales, the development of high-precision controllable fabrication technologies, as well as the evaluation of safety and stability for clinical and industrial translation.[16-18]

As the first cross-field systematic review focusing on curvature-tailored nanocarriers, this study is not a simple integration of curvature-related research in various sub-fields or renaming of existing topics, but forms clear differentiation and complementarity with existing studies: First, different from reviews focusing on the overall morphology/shape of nanomaterials, this review breaks through the limitation of qualitative description of geometric features in traditional morphological research, and for the first time elevates curvature from an "auxiliary morphological feature" to an independent core functional regulatory parameter, constructing a complete and universal technical system from curvature type classification, precise quantitative characterization to controllable synthesis. Second, different from the fragmented discussion of curvature in sub-fields such as protein corona and single-atom catalysis, this review for the first time systematically explores the cross-field common mechanisms (surface stress regulation, electronic structure reconstruction, interfacial interaction optimization) of curvature in regulating functions in three major fields: biomedicine, catalysis, and material assembly, and establishes a quantitative correlation between curvature and its "structure-performance". Third, this review combs the technical bottlenecks and common challenges of curvature regulation in different fields for the first time, providing a unified methodological guidance for cross-field curvature engineering research, and filling the gap in systematic reviews of curvature as a core design dimension for nanomaterials. Centering on the core concept of curvature as a

functional modulation dimension, we have systematically conducted a full-chain research spanning theoretical design, controllable synthesis, multi-scale characterization, and functional applications.[19-22] It aims to establish the rational design principles of curvature-tailored nanocarriers, develop methods for their precise fabrication and quantitative evaluation, reveal the physicochemical mechanisms underlying the effects of curvature on carrier functions, and explore their application prospects in major disease treatment, green energy catalysis, and advanced smart materials (**Figure 1**). Through the implementation of this research, we anticipate providing systematic theoretical support and methodological tools for the development of curvature nanotechnology, and driving the evolution of nanotechnology toward the next phase of on-demand functional customization.[23,24]

2. Design and synthesis strategies of curvature-tailored nanocarriers

2.1 Curvature types and geometric parameterization

The design of curvature-tailored nanocarriers first requires clarifying the curvature types and corresponding geometric parameters. Based on geometric characteristics, curvature can be categorized into three fundamental types: positive curvature, negative curvature, and mixed curvature (**Figure 2**). Positive curvature structures include nanospheres, nanorods, nanostars, and nano-onions, where the mean curvature at any point on the surface is positive. Negative curvature structures cover nanocages, nanobowls, and porous frameworks, which possess local or global regions with negative curvature on the surface. Mixed curvature structures refer to complex geometries that exhibit both positive and negative curvature features simultaneously, such as dumbbell-shaped, peanut-shaped, and disk-pore composite structures. There is a clear geometric quantitative relationship between curvature and the size of nanocarriers. For the typical regular morphology nanocarriers involved in this study, their curvature can be directly quantified by characteristic sizes: the mean curvature of positively curved spherical nanoparticles is $H=1/R$ (R is the particle radius), with smaller particle sizes corresponding to larger curvatures; the mean curvature

of negatively curved hollow hemispheres is $H=-1/r$ (r is the concave curvature radius), and the mean curvature of carbon nanotubes is $H=1/D$ (D is the tube diameter), with smaller characteristic sizes corresponding to larger absolute values of curvature. For complex mixed curvature carriers, the local curvature can be quantified separately by the characteristic sizes of the corresponding regions, which provides a geometric basis for the precise characterization and regulation of curvature.

In terms of geometric parameterization, it is necessary to establish a unified curvature description system. For simple geometries, the mean curvature H and Gaussian curvature K can be employed as the basic parameters. The mean curvature is defined as the average value of the two principal curvatures, reflecting the degree of surface bending; the Gaussian curvature is the product of the two principal curvatures, characterizing the local geometric properties of the surface. For the typical positive and negative curvature nanocarriers involved in this study, the analytical calculation formulas of H and K are as follows: (1) Spherical nanoparticles (positive curvature): $H=1/R$, $K=1/R^2$ (R is the particle radius); (2) Carbon nanotubes (positive curvature): $H=1/D$, $K=0$ (D is the tube diameter); (3) Hollow hemispheres (negative curvature, nanobowls): $H=-1/r$, $K=1/r^2$ (r is the concave curvature radius, the negative sign identifies negative curvature). For simple geometries (e.g., nanospheres, nanotubes), H and K can be directly calculated via analytical formulas; for complex mixed curvature structures, parameter extraction needs to be achieved by combining image processing and geometric modeling.[25-28]

2.2 Curvature characterization

Accurate measurement of curvature is fundamental to understanding curvature effects and optimizing synthetic processes. Currently, a variety of high-resolution characterization techniques have been developed, tailored to different application scenarios. These can be primarily categorized into three major classes: microscopic imaging, scattering-based methods, and modeling-analysis approaches, each with its unique advantages and scope of applicability (**Table 1**).

Electron microscopy is the most intuitive and widely used technique for curvature characterization, as it directly captures high-resolution images of nanocarrier morphologies and extracts curvature parameters through image processing. Transmission electron microscopy (TEM) and scanning electron microscopy (SEM) provide nanoscale-resolution 2D morphological observations, making them suitable for measuring curvature in most types of nanocarriers, such as nanospheres, nanotubes, and nanobowls. For example, SEM images can be used to directly measure the diameter of nanospheres, from which the average curvature can be calculated. TEM cross-sectional views of nanotubes allow for the determination of the negative curvature of their inner walls.[29,30] Cryogenic electron microscopy (cryo-TEM) enables the observation of carrier structures under near-physiological solution conditions, avoiding potential morphological distortions caused by drying or staining processes. This makes it particularly suitable for characterizing curvature in biocompatible carriers such as lipid vesicles and polymer micelles.[31]

Small-angle scattering techniques can characterize the overall curvature distribution and assembly state. These techniques include small-angle X-ray scattering (SAXS) and small-angle neutron scattering (SANS).[32] By analyzing the characteristic peaks and intensity distribution in the scattering patterns, the overall curvature distribution, size uniformity, and assembly structure of the carriers can be inferred. Their key advantage lies in the ability to perform measurements in solution, which closely reflects the actual application environment of the carriers.

Atomic force microscopy (AFM) simultaneously acquires three-dimensional morphological and mechanical correlation information. By scanning the sample with a probe, AFM achieves high-resolution imaging of the three-dimensional morphology of carriers, enabling not only the extraction of curvature parameters but also the concurrent measurement of local mechanical properties, thereby indirectly revealing the relationship between curvature and material mechanical performance.[33] AFM can be performed in various environments, such as air or solution, making it suitable for in situ characterization of biological carriers. With resolution reaching the atomic scale, it can precisely

capture local curvature variations at the nanoscale (e.g., high-curvature regions at the tips of nanostars). It is commonly used to verify the curvature uniformity of synthesized carriers and to study the influence of curvature on the mechanical properties of carrier surfaces.[34] Extended X-ray absorption fine structure (EXAFS) is a key spectral characterization technology widely used in the study of curvature-regulated catalytic systems. This technology can accurately analyze the local atomic coordination environment, bond length and bond angle of metal active sites on the surface of curved carriers by detecting the fine structure of X-ray absorption spectra. The characteristic peak position, intensity and shape in the EXAFS spectra can directly reflect the curvature-induced lattice strain and electronic structure changes of active sites, and provide atomic-scale structural evidence for revealing the regulatory mechanism of curvature on catalytic performance. This technology is often combined with Fourier transform and density functional theory calculation for data analysis, and its test results are important for verifying the structural optimization effect of curvature on catalytic active sites as shown in subsequent figures.

For mixed curvature structures with complex morphologies, it is necessary to combine image processing software for digital modeling, and then calculate curvature parameters via geometric algorithms. The core workflow is as follows: first, acquire 2D/3D images using techniques such as TEM and AFM; second, perform denoising, segmentation, and contour extraction on the images to construct a digital model of the carrier; finally, obtain the distribution maps of mean curvature and Gaussian curvature using curvature calculation algorithms. This method enables the accurate quantification of curvature for complex structures, providing data support for the optimization of synthesis processes.[35] The core contradiction of various characterization techniques lies in the incompatibility among resolution, in-situ performance, and applicability: High-resolution techniques (TEM/AFM) are difficult to achieve in vivo in-situ characterization, while in vivo imaging techniques (fluorescence imaging) cannot accurately quantify curvature. Cryo-TEM serves as the

"ideal approach" but is limited by high cost. These represent the key bottlenecks that urgently need to be broken through for curvature characterization techniques.

2.3 Synthetic methods for precise curvature regulation

Precise curvature regulation constitutes a key technology for the functionalization of curvature-tailored nanocarriers. A variety of effective synthetic strategies have been developed to date, primarily including the template method, self-assembly method, controlled buckling method, and etching method.

The template method guides material growth using templates with specific sizes and shapes; the carriers with target curvature can be obtained after template removal. Its core advantages lie in the precise controllability of curvature size, uniform morphology, and suitability for large-scale production. Template methods can be categorized into hard-template and soft-template approaches based on the template material.[36-38] The hard-template method employs rigid materials (e.g., polystyrene (PS) spheres, ZnO rods, and metal-organic frameworks (MOFs) as templates. The target materials are coated on the template surface via sol-gel, chemical deposition, and other techniques, followed by template removal through etching, high-temperature calcination, and analogous processes. The soft-template method utilizes flexible structures such as surfactant micelles and block copolymer micelles as templates, leveraging intermolecular interactions to direct the oriented growth of materials[39-41].

The self-assembly method utilizes non-covalent intermolecular interactions and thermodynamic driving forces to enable the spontaneous formation of structures with specific curvature. This synthesis process is mild and does not require complex equipment, making it suitable for producing biocompatible carriers.[42] Block copolymer self-assembly can be tuned by adjusting solvent ratios and polymer concentrations to induce the formation of vesicles and cylindrical structures with varying curvatures. Lipid self-assembly is a process in which amphiphilic lipid molecules, driven by

hydrophobic interactions in aqueous environments, spontaneously form ordered supramolecular structures.[43]

The controlled buckling method induces controllable material buckling by adjusting parameters such as interfacial tension and solvent evaporation rate, thereby forming structures with specific curvature.[44] Microfluidic technology serves as a key enabler for this method, allowing for high-precision and scalable control of curvature. The core principle involves using microfluidic chips to precisely regulate droplet formation and interfacial tension, enabling droplets to adopt specific curvatures. The desired shape is then fixed via solvent evaporation or chemical cross-linking, resulting in the formation of polymer carriers.[45]

The etching method uses solid nanoparticles as precursors to construct negative curvature structures by creating depressions or pores on the surface through selective etching. This technique allows for secondary processing based on existing structures, enabling fine tuning of curvature with high precision, making it particularly suitable for fabricating porous negative-curvature carriers.[46] For example, solid SiO_2 nanospheres can be used as precursors and selectively etched with hydrofluoric acid (HF) solution. By controlling the etching time and HF concentration, the depth and shape of the depressions can be adjusted, achieving precise regulation of negative curvature. Additionally, combining this method with hard-template-assisted strategies (such as sol-gel or chemical vapor deposition) enables accurate control over the concavity and convexity of nanoparticles through a "template precursor preparation-target material deposition-template removal" process, meeting diverse functional requirements.[47] In summary(**Table 2**), the core trade- offs among existing synthetic methods center on three factors: curvature control precision, scalability of preparation, and cost. The self- assembly approach offers high scalability but suffers from poor curvature controllability. Microfluidics and 4D printing enable precise curvature regulation yet are limited by equipment requirements and cost. The template method serves as a compromise solution

but carries the risk of impurity introduction. These aspects represent the key optimization directions for future synthesis technologies of curvature- engineered nanocarriers.

The core common challenge of current synthesis techniques for curvature- engineered nanocarriers lies in the dual deficiency of precise quantitative design and dynamic reversible regulation of curvature: most synthesis methods only achieve qualitative control over curvature and cannot realize accurate quantitative design. Meanwhile, static curvature carriers are difficult to adapt to the requirements of in vivo or dynamic application scenarios, and dynamic curvature regulation technologies are still limited by material types and fabrication costs. Furthermore, the regulation laws of curvature vary significantly among different material systems, and a unified synthetic design principle has not yet been established, which is also the main reason why curvature regulation technologies are difficult to apply across fields.

3. Performance evaluation for diverse application scenarios

3.1 Drug delivery and therapeutic applications

With its precise ability to regulate biointerface interactions through unique geometric structures, curvature nanocarriers have evolved into a promising novel functional platform, demonstrating advantages in improving drug targeting, enhancing delivery efficiency, and strengthening therapeutic efficacy.[48] Their core value lies in providing innovative and efficient solutions for three core application scenarios, drug delivery, anti-tumor therapy, and vaccine development and immune activation, by regulating key mechanisms such as active center structure, intracellular endocytic pathways, and drug-carrier interaction modes, thus emerging as a research frontier and hotspot in the field of nanobiomedicine.[49]

In the field of drug delivery, the core advantage of curvature nanocarriers is their ability to precisely modulate their own structures according to the physicochemical properties of different drugs, break through multiple physiological barriers such as intracellular delivery, conformational

protection, and tissue penetration, comprehensively improve delivery efficiency, and provide customized solutions for the efficient delivery of various types of drugs. Among these, in the key step of intracellular delivery of nanomedicines, silica nanoparticles with human serum protein corona play an irreplaceable regulatory role.[50] Through the specific binding of surface serum protein corona to cellular LDL receptors, the carriers bypass the traditional clathrin-mediated endocytosis; instead, they activate BAR domain proteins centered on BIN1 and GRAF1 (**Figure 3a**), and coordinate with their own physical curvature to drive membrane bending, thus achieving internalization via multiple clathrin-independent endocytic pathways including dynamin-dependent and caveolin-mediated routes.[51,52] Notably, the delivery efficiency of 50 nm high-curvature carriers is significantly superior to that of large-sized low-curvature counterparts. This high-efficiency delivery originates from the synergistic effect between carriers and intracellular curvature sensing proteins, which not only overcomes the pathway limitations of traditional receptor-mediated endocytosis, but also provides a specific regulatory pathway through the curvature-dependent protein activation effect (**Figure 3b**), laying a core foundation for optimizing the delivery mechanism of targeted nanomedicines. Moreover, curvature also regulates the endosomal escape efficiency of nanocarriers, a key step for bioactive drugs (e.g., nucleic acids, proteins) to exert functions in the cytoplasm. High-curvature carriers can induce endosomal membrane destabilization by modulating lipid raft aggregation and membrane tension, thereby promoting drug release into the cytoplasm—a mechanism that has been verified in silica and polymer-based nanocarrier systems.[53]

Beyond nanomedicines, curvature carriers also exhibit outstanding performance in the delivery of bioactivity-sensitive peptide drugs, and play a crucial regulatory role especially in the conformational protection and efficient delivery of α-helical peptide drugs. Studies have demonstrated that carbon nanotubes with small diameters and high curvatures, such as (10,10) CNTs, serve as delivery systems with advantages, which can effectively maintain the conformational stability of the α-helix structure of exenatide (EXN) and ensure the bioactivity of the drug.[54,55] This

effect stems from the unique structure of high-curvature carriers: their small diameters restrict excessive contact between peptide chains and the carriers, thereby preventing peptide chain unfolding caused by excessively strong van der Waals interactions; meanwhile, they balance the contact area and interaction strength to protect the intramolecular hydrogen bond network of peptide chains (**Figure 3c**). In contrast, carriers with large diameters (low curvatures) tend to induce peptide chain spreading and α-helix structure destruction due to their large adsorption areas, thus reducing delivery effectiveness (**Figure 3d**). By precisely regulating the drug-carrier interaction mode, high-curvature carriers provide core support for the efficient delivery of α-helical peptide drugs.

In enhancing the delivery efficiency of drugs to deep pathological tissues, high-curvature carriers with specific morphologies demonstrate breakthrough advantages. Among them, the high-curvature spindle-shaped nanoparticle ENP5 (tip mean curvature: 0.04~0.05 nm^{-1}, corresponding to a tip curvature radius of 20~25 nm) significantly outperforms traditional spherical, rod-shaped, and small spherical particles in delivery efficacy (**Figure 3e**).[56,57] Its core advantage stems from the precise regulation of key delivery stages by high curvature: during the extravasation stage, the high-curvature tips compress fluid space, suppress turbulence and backflow, and reduce fluid resistance, thereby overcoming the pressure gradient barrier formed by high interstitial fluid pressure (IFP) in tumors, enabling rapid extravasation from blood vessels into the tumor interstitium (**Figure 3f**); during the penetration stage, high-curvature-driven rapid rotation increases the carrier hopping frequency, allowing it to efficiently escape entanglement by the dense extracellular matrix (ECM) and deeply penetrate toward the tumor core. Ultimately, high-curvature carriers optimize the entire extravasation-penetration process, achieving efficient drug enrichment within tumors, laying a critical foundation for therapy, and providing an innovative solution for drug delivery to pathological tissues with high IFP.

In the scenario of tumor-targeted therapy, curvature nanocarriers effectively address the core challenges of low tumor inhibition rate and poor targeting of traditional nanocarriers through

structural regulation strategies such as enhancing the function of active sites and optimizing the accessibility of targeting ligands, thereby significantly improving the precision and effectiveness of anti-tumor therapy.[58] In nanozyme-mediated tumor therapy, the diatomic nanozyme C-Fe_1Cr_1NC supported by high-curvature nitrogen-doped carbon carriers exhibits excellent anti-tumor performance. When combined with ascorbic acid (AA), it achieves a tumor inhibition rate of 62.0% in 4T1 breast cancer mice in vivo, which is significantly superior to the non-curvature carrier group (44.4%) and the AA monotherapy group (15.4%) (**Figure 4a**). The tumor growth curves in the figure directly reflect the dynamic inhibitory effect of different treatment groups on tumor progression, and the slowest tumor growth in the high-curvature carrier group fully verifies its in vivo therapeutic superiority. In vitro, the killing rate of 4T1 cells reaches 70%, far exceeding that of the single-atom and planar carrier combinations. This system has good biocompatibility without obvious systemic toxicity. The performance stems from the structural advantages of high-curvature carriers: on the one hand, it enhances the AO-like, POD-like, and GSHOx-like activities of nanozymes by modulating the electronic structure of metal active centers, shortening the Fe-Cr distance, and increasing the specific surface area (**Figure 4b**). The UV-vis absorption spectra of AA oxidation in the figure intuitively characterize the catalytic activity of different nanozyme systems, and the significant absorption peak change of the C-Fe_1Cr_1NC group indicates the strongest oxidation capacity of the high-curvature regulated active sites. On the other hand, it drives cascade reactions in the tumor microenvironment, oxidizes AA to in situ generate H_2O_2 and a large amount of ROS, consumes GSH, and synergistically induces tumor cell apoptosis through oxidative stress and lipid peroxidation, ultimately achieving efficient anti-tumor effects.

Beyond nanozyme systems, curvature carriers also demonstrate significant advantages in targeted molecularly modified antitumor delivery systems. A typical example is the DNA-gold nanostar (DNA-AuNS) curvature carrier, which provides crucial support for efficient antitumor therapy.[59] Its high positive curvature tips (<10 nm) can reduce the adsorption density and uniformity

of serum protein corona, endowing the carrier with a differentiated "biological identity" in the biological microenvironment; this unique identity not only preserve the targeting function of surface anti-HER_2 aptamers (HApt) in biological environments, ensuring specific binding to HER_2 receptors on tumor cell surfaces, but also prolongs the blood circulation time by reducing opsonization and subsequent clearance by the mononuclear phagocyte system.[59] This dual effect lays the foundation for inducing receptor lysosomal degradation and inhibiting tumor proliferation. Its excellent targeting performance stems from the high positive curvature tips (<10 nm): the spatial steric hindrance effect reduces the adsorption and shielding of serum protein corona, allowing targeting ligands to bind more easily to tumor cell receptors (**Figure 4c**). The negative-stained TEM images and corresponding binary images in the figure clearly show the distribution difference of protein corona on the surface of spherical nanoparticles and high-curvature gold nanostars, and the sparse protein corona on the tip of gold nanostars directly reflects the shielding reduction effect of high curvature. Moreover, compared to traditional spherical nanocarriers, the curvature-mediated uneven protein corona distribution further enhances ligand accessibility (**Figure 4d**). The quantitative analysis of protein corona coverage in the figure intuitively verifies that high curvature can significantly reduce the non-specific adsorption of serum proteins, thus improving the effective exposure of targeting ligands. This characteristic also significantly reduces non-specific uptake by liver Kupffer cells, thereby improving tumor-targeted accumulation efficiency while decreasing off-target organ distribution in the liver and other normal tissues. This overcoming the core bottleneck of protein corona interference in targeted nanodrug delivery and strengthening the antitumor effect.

In the field of vaccine development and immune activation, curvature nanocarriers can utilize cell membrane curvature modulation to construct an integrated "delivery-adjuvant" system, effectively overcoming the limitation of weak immunogenicity of single antigens. This provides a novel technical pathway for the efficient development of therapeutic vaccines. The application of this approach has been validated in specific carriers, with the curvature carrier Qβ NP (Qβ virus-like

particle) demonstrating exceptional value.[60,61] This protein-based curvature nanocarrier conforms to the functional modification strategy of protein nanocages for drug delivery systems[61], laying a structural and methodological foundation for the design of curvature-based vaccine carriers. The antihypertensive vaccine ATR-NP constructed using this carrier exhibits potent immune activation effects, inducing high-titer specific antibodies against AT1R, significantly increasing the expression of CD80 and MHC-II molecules on the surface of dendritic cells (DCs), and promoting the differentiation of Th1 and Tfh cells, thereby providing strong support for B cell activation and antibody production. This efficacy originates from the curvature properties of Qβ NP, by modulating cell membrane curvature through electrostatic adsorption, it drives the aggregation and reorganization of lipid rafts and reduces their diffusion rate, forming a stable signal transduction platform. This further promotes the enrichment and phosphorylation of signaling proteins within lipid rafts, enhancing immune signal transduction (**Figure 4e**). The quantitative detection results of Src and pSrc accumulation in lipid raft domains in the figure directly reflect that curvature carriers can significantly promote the phosphorylation and enrichment of immune signaling proteins, thus amplifying the intracellular immune signal transduction cascade. This mechanism overcomes the bottleneck of weak immunogenicity of single antigen peptides and offers an efficient integrated strategy of delivery vehicle and immune adjuvant for the development of therapeutic vaccines.

As a design parameter for drug delivery carriers, curvature presents significant trade-offs and contradictory research findings. On the one hand, high-curvature carriers can enhance targeted delivery efficiency by reducing protein corona adsorption and improving ligand accessibility. On the other hand, some studies have confirmed that excessive surface curvature can induce conformational unfolding of protein molecules, which not only impairs the function of targeting ligands on the carrier surface but may also expose hydrophobic regions of proteins, triggering non-specific immune responses and leading to rapid clearance of carriers by the mononuclear phagocyte system. This constitutes the core contradiction in the in vivo application of high-curvature carriers. In addition,

practical challenges in curvature regulation include: the complex biological microenvironment in vivo (such as pH and ionic strength) can alter the apparent curvature of carriers, resulting in the failure of curvature performance designed in vitro to function effectively in vivo. Meanwhile, the coupling effects between curvature and carrier size, surface charge are difficult to decouple, making it impossible to independently evaluate the actual regulatory role of curvature. These remain key issues to be addressed in future research in this field.

3.2 Structure-activity relationship in catalytic applications

As a core structural engineering tool for regulating catalyst performance, curvature supports rely on their unique geometric bending characteristics to precisely manipulate catalytic processes from multiple dimensions, including electronic structure, reaction kinetics, reaction mechanism, and coordination environment, thereby breaking through the bottlenecks of traditional planar supports in performance optimization.[62,63] In contrast to conventional size and composition regulation strategies for catalysts, curvature engineering exhibits irreplaceable advantages: size optimization improves catalytic activity primarily by increasing specific surface area and exposing more active sites, yet it is limited by nanosized active site agglomeration and reduced structural stability; composition modification optimizes active site chemical properties via doping, alloying or atomic substitution, but it often increases preparation complexity and cost, and may cause uneven distribution of active sites. Curvature regulation, however, modulates catalytic performance from a structural perspective by inducing microstrain and reconstructing active site electronic structure, without changing the catalyst's chemical composition or relying on specific surface area enhancement, enabling precise tuning of intermediate adsorption energy and reaction pathways that are difficult to achieve via size or composition adjustment alone. Their core value lies in comprehensively optimizing the electronic states of active sites, the adsorption strength of intermediates, reaction energy barriers, and product growth pathways through key effects such as curvature-induced microstrain, local electric field regulation, and charge distribution reconstruction. This provides innovative strategies and core

support for the rational design of highly efficient, stable, and highly selective catalysts, especially single-atom catalysts and demonstrates irreplaceable application potential in various catalytic fields, emerging as one of the key directions in current catalytic material research.[64-66]

The electronic structure is the core factor determining catalyst activity. Curvature supports can achieve precise reconstruction of the electronic states of active sites by constructing unique geometric microenvironments, thereby significantly enhancing catalytic performance.[67] Studies have found that concave carbon supports with high surface curvature break the symmetric electron distribution of planar Fe-N_4 sites by inducing intrinsic microstrain, while shortening the Fe-N bond length, which lays a geometric foundation for electronic structure reconstruction (**Figure 5a**).[68] The k^3-weighted Fourier-transformed Fe K-edge EXAFS spectra of Fe SA/NhcC and Fe SA/NC show obvious characteristic peak shifts compared with the reference samples of Fe foil and Fe_2O_3. The reduction of the main peak intensity and the shift of the peak position directly indicate that curvature induces the shortening of Fe-N bond length and the change of local coordination environment of Fe atoms. This curvature effect drives the spatial redistribution of charges between Fe atoms and the surrounding N and C atoms, reduces the electron loss of Fe atoms, optimizes the electronic states of active sites, lowers the charge transfer resistance, and improves electron transfer efficiency (**Figure 5b**). More importantly, curvature significantly downshifts the d-band center of Fe through strain effects, avoiding the problem of excessively strong adsorption of oxygen-containing intermediates, while moderately regulating the *OOH adsorption energy to keep the intermediate binding strength within the optimal catalytic range (**Figure 5c**). It is this comprehensive regulation of electronic structure that endows Fe SA/NhcC with bifunctional catalytic activity.

Carriers with well-defined high-curvature structures, such as carbon nano-onions (CNOs), exhibit unique advantages in charge injection and selective distribution. The distinctive high-curvature structure of CNOs first leads to a significant reduction in the thickness of the electric double layer (EDL), decreasing by approximately two-thirds compared to planar carriers. Based on

capacitive characteristics, this results in a several-fold improvement in the charge injection efficiency of the system, laying the foundation for electronic structure regulation (**Figure 5d**).[9] High curvature selectively regulates charge distribution, enabling the key CO_2 reduction intermediate COOH to acquire more additional charge than the competing H species (**Figure 5e**). Crystal orbital Hamiltonian population analysis reveals that the injected charge equally strengthens bonding interactions. However, the greater charge increment for COOH selectively enhances its adsorption to the Zn-N_4 active center, thereby optimizing the adsorption free energy difference of intermediates (**Figure 5f**). This comprehensive regulation of electronic structure from charge injection and distribution to adsorption interactions, ultimately leads to a leap in catalytic selectivity and activity, highlighting the core value of curvature carriers in electronic structure optimization.

While the aforementioned studies largely focus on single-atom catalyst systems, the curvature effect also exhibits significant specificity and differentiation in regulating the electronic structures of composite active phases such as metal carbides. Curvature serves as a key carrier factor in modulating the electronic structure of MoC_y/C-based catalysts. Through geometric differences between concave and convex surfaces as well as variations in curvature magnitude, it precisely adjusts the interaction between MoC_y nanoparticles and the carbon support, thereby reshaping the electronic structure (**Figure 5g**).[69] In concave regions, as the curvature of the carrier increases, the adsorption strength of MoC_y enhances linearly, and electron transfer from MoC_y to the carbon support becomes more pronounced. This results in nanoparticles exhibiting a stronger positive charge state, with more prominent electron accumulation and depletion effects at the interface, and an increased degree of electron cloud overlap in the Mo-C chemical bonds. This curvature-dependent regulation essentially optimizes the electronic environment of the active sites (low-coordination Mo atoms) by altering the electron cloud distribution on the carbon carrier surface and the adsorption configuration of MoC_y. Ultimately, the differentiated adjustments in electronic structure directly influence catalytic performance. For instance, MoC_y loaded on convex surfaces demonstrates

stronger electron-donating capability and superior efficiency in CO_2 adsorption and activation, providing a precise pathway for electronic structure regulation in the rational design of catalysts.

Beyond electronic structure regulation, the efficiency of reaction kinetics serves as a critical underpinning for enhanced catalytic performance. Curvature supports can significantly accelerate the reaction kinetic process by modulating core factors such as the local microenvironment, intermediate transfer, and reaction energy barriers.[70] Onion-like carbon nanospheres (OLCs) with high curvature act as core carriers for reaction kinetics regulation. Their curved surfaces generate a tip-enhanced local electric field (**Figure 6a**), which not only enriches protons to accelerate their transfer toward Pt active sites (**Figure 6b**) but also precisely optimizes the hydrogen adsorption free energy. This drives the reaction to follow the Volmer-Tafel mechanism, with *H recombination as the rate-determining step, thus boosting the kinetic rate (**Figure 6c**).[71] This catalyst delivers an overpotential of merely 38 mV at 10 mA cm^{-2}, a Tafel slope of 36 mV dec^{-1}, along with excellent stability over 100 h. These results provide a crucial reference for the precise regulation of HER reaction kinetics via curvature engineering and the design of high-efficiency single-atom catalysts.

The kinetic optimization effect of curvature supports is not limited to two-electron transfer reactions such as the hydrogen evolution reaction (HER); their regulatory role is equally prominent in oxygen reduction reactions (ORR) involving multi-electron transfer as well as in the applications of energy storage devices.[72] By precisely modulating reaction kinetics (**Figure 6d**), chiral curved carbon nanospheres (CCNs) with high curvature enable the Fe single-atom-supported catalyst (Fe/CCNs) to exhibit catalytic performance far superior to that of curvature-free Fe/CNs and commercial Pt/C catalysts.[58] The core mechanism lies in the directional regulation of key ORR kinetic steps by curvature supports: curvature-induced local strain and interfacial electric fields significantly weaken the excessively strong adsorption between Fe-N_4 sites and *OH, thus drastically reducing the *OH desorption energy barrier, the overpotential of concave Fe sites is merely 0.48 eV, which is far better than that of planar counterparts. Meanwhile, it optimizes the electronic structure

of Fe to achieve an efficient four-electron transfer pathway; additionally, it balances intermediate adsorption-desorption behaviors by regulating the orbital interaction between Fe and O, which is in line with the Sabatier principle. Ultimately, the Fe/CCNs catalyst achieves an ORR half-wave potential of 0.89 V (**Figure 6e**), with a kinetic current density exceeding that of Pt/C. The liquid zinc-air battery assembled with this catalyst delivers a peak power density of 162.7 mW cm^{-2} and maintains stable cycling for 250 h, while the flexible battery achieves a peak power density of 122.1 mW cm^{-2} and endures bending for 40 h (**Figure 6f**). These results demonstrate that curvature supports realize a improve in catalytic performance by regulating reaction energy barriers, electron transfer, and adsorption-desorption kinetics, providing a core strategy for the kinetic optimization of single-atom catalysts.

Extending from electrocatalytic systems to advanced oxidation systems, curvature supports can also achieve a substantial enhancement in kinetic efficiency by regulating the generation pathways of reactive species. By tailoring the particle size of hollow porous carbon spheres, the constructed PCN-FeSA catalyst series exhibits distinct curvature-dependent kinetic characteristics. Through modulating the electronic structure of Fe active sites, curvature shifts the d-band center toward the Fermi level, which significantly reduces the peroxymonosulfate (PMS) adsorption energy (-2.28 eV) and enhances interfacial charge transfer efficiency (**Figure 6g**), thus accelerating the kinetics of O-O bond cleavage and activation.[73] Such regulation also governs the transformation of reactive oxygen species (**Figure 6h-i**): the high-curvature system takes $^1O_2$ as the dominant reactive species, with a generation rate 22–77 times higher than that of the low-curvature system, forming an efficient non-radical oxidation pathway; in contrast, the low-curvature system is dominated by high-valent metal-oxygen species, leading to a marked decline in kinetic efficiency. Ultimately, the high-curvature catalyst achieves complete degradation of ciprofloxacin within 10 minutes with a utilization efficiency of 57.8%. These results verify that curvature enables a leapfrog improvement in catalytic performance by optimizing key kinetic steps such as adsorption, charge transfer, and reactive species

The precise regulation of catalytic reaction mechanisms represents a fundamental strategy for achieving breakthrough improvements in catalytic performance. Curvature carriers enable this by creating differentiated local microenvironments, fundamentally altering reaction pathways, intermediate evolution, and product growth patterns. Using high-curvature onion-like carbon spheres (OCS) and low-curvature reduced graphene oxide (rGO) as carrier models[74], theoretical calculations confirm that high-curvature structures induce charge accumulation at curvature extremal regions due to the tip effect, forming a strong localized electric field that reduces the adsorption energy of intermediates such as LiO_2 and $(Li_2O_2)_2$. This guides the growth of Li_2O_2 in a bottom-up columnar array (**Figures 7a-b**). In contrast, low-curvature carriers exhibit uniform charge distribution, which tends to cause intermediate instability and dense film-like agglomeration of products. In situ tests further validate that on high-curvature carriers, reaction intermediates are continuously enriched, charge transfer resistance is lower, and side reactions are effectively suppressed, whereas low-curvature carriers exhibit chaotic reaction pathways (**Figure 7c**). This mechanistic regulation enables Ru SACs/OCS-catalyzed Li-O_2 batteries to achieve an ultrahigh discharge capacity of 25608 mAh g^{-1}, a low overpotential of 0.52 V, and long-term cycling stability over 2000 h, far surpassing the performance of low-curvature carrier systems. These results fully demonstrate the core value of curvature carriers in enhancing catalytic performance through precise control of reaction mechanisms.

Curvature support serves as the core for regulating the ORR mechanism of curved-surface Fe/N-C (CS Fe/N-C) catalysts. By virtue of its unique multi-layer graphitized hollow nano-protrusion structure, it fundamentally optimizes the reaction pathway and the stability of active sites.[75] There exists a selective electrostatic repulsion between the outer N-doped carbon layer and the inner oxygenated intermediates (**Figure 7d**). Owing to the differences in the charge characteristics and spacing of intermediates, the repulsive force can be regulated over a wide range, which breaks the linear scaling relationship between ΔG_{*O} and ΔG_{*OOH} (**Figure 7e**). This

significantly weakens the excessive adsorption of intermediates and addresses the bottleneck of limited activity in planar catalysts. Meanwhile, the curvature configuration alters the microenvironment of Fe active sites, modulates the relative strength of O-O and O-Fe bonds (**Figure 7f**), and drives the ORR to preferentially follow the $4e^-$ pathway, thereby reducing the generation of hydroxyl radicals. This series of mechanism regulations endows the catalyst with excellent performance: the calculated ORR overpotential is merely 0.34 V; the H_2-air proton exchange membrane fuel cell (PEMFC) achieves a peak power density of 0.75 W cm^{-2} at 1.0 bar; and the activity retention rate remains at 86% after 300 hours of operation, realizing the synergistic enhancement of activity and stability.

Curvature carriers serve as a core strategy for regulating the reaction mechanisms of SACs, essentially optimizing catalytic performance through the modulation of intermediate binding energies. A smaller carrier diameter (i.e., greater curvature) results in a stronger interfacial electric field, which can uniformly act on all active sites, overcoming the issue of uneven electric field distribution in traditional tip-based structures (**Figure 7g**).[76] The electric field enables precise adjustment of intermediate binding energies based on their dipole moments and polarizabilities, optimizing the free energy barrier of the rate-determining step while breaking the scaling relations limitations of conventional catalysis (**Figure 7h**). In acidic CO_2 reduction, the optimally curved Ni-SAC-250 stabilizes the *COOH via the electric field, lowering the energy barrier of the rate-determining step and achieving a CO partial current density of 400 mA cm^{-2} with >99% Faraday efficiency. In alkaline ORR, the strong electric field of Fe-SAC-70 optimizes OOH/OH binding energies, leading to a half-wave potential of 0.91 V. This strategy provides a universal pathway for mechanistic regulation across various electrocatalytic reactions.

The coordination environment of active sites constitutes the fundamental guarantee for catalytic performance. Curvature supports can modulate the metal coordination bond structure, electronic state, and stability via inducing strain effects, thereby optimizing catalytic activity and selectivity.[77] In the

study, nitrogen-doped defect-rich carbon nano-onions (CNOs) with positive Gaussian curvature were employed as the support. They anchored iron phthalocyanine (FePc) through π-π stacking, inducing a square planar symmetry distortion of the Fe-N_4 coordination with D_4h symmetry (**Figure 8a**), and facilitating the transformation of Fe^{2+} from a low-spin state to an intermediate-spin state (**Figure 8b-c**).[78] The Fourier-transformed Fe K-edge EXAFS spectra show that the characteristic peak of FePc/CNOs at the Fe-N bond position has a significant shift and broadening compared with pure FePc, which directly reflects the curvature-induced distortion of the Fe-N_4 square planar coordination structure and the change of bond length. This curvature-induced strain regulates the energy levels and electron distribution of Fe *d* orbitals, weakens the excessive adsorption of oxygen intermediates on Fe-N_4 sites, promotes O_2 activation and *OH desorption, and thus significantly enhances the ORR activity as well as the catalytic performance of zinc-air batteries.

The high-curvature tubular B,N-co-doped carbon carrier RuBNC2000 demonstrates breakthrough advantages, with its core strengths stemming from the precise regulation of key catalytic steps by high curvature. During the coordination bond modulation stage, the high-curvature carrier surface induces local strain, compressing Ru-N bonds by 1.5% and stretching Ru–B bonds by 4%. This avoids excessively strong or weak coordination interactions and constructs an optimal RuN_2B_1 active site configuration (**Figure 8d**). The R-space EXAFS curves of RuBNC2000 show that the characteristic peaks of Ru-N and Ru-B bonds have obvious position shifts compared with RuBNC8000 and reference samples of RuO_2 and Ru foil, and the peak intensity change further verifies the curvature-induced bond length adjustment and the formation of the RuN_2B_1 coordination structure. Moreover, Ru species are highly dispersed in both carriers without agglomeration interference, providing a structural foundation for coordination regulation (**Figure 8e**).[79] In the electronic structure optimization stage, curvature-driven bond length adjustments promote positive charge accumulation at Ru sites and quench spin polarization, precisely optimizing *H adsorption strength in line with the Sabatier principle. This electronic state alteration can be intuitively verified

through absorption edge shifts. The high-curvature carrier achieves efficient catalysis under ultra-low Ru loading (0.4 wt%), with its catalytic activity clearly demonstrated in polarization curves. Both the overpotential and reaction kinetics significantly outperform those of low-curvature carriers and Pt/C (**Figure 8f**), while also exhibiting excellent stability. This lays a crucial foundation for the design of efficient HER catalysts and offers an innovative strategy for active site regulation in single-atom catalysts.

The application of curvature regulation in catalysis focuses on the core trade-off between catalytic activity and catalyst stability. High-curvature/high-strain catalytic interfaces can significantly enhance catalytic activity by tuning adsorption energies of reactants and optimizing reaction pathways. However, excessive curvature induces overly large lattice strain in catalytic materials, accelerating catalyst agglomeration and degradation, thus reducing cycling stability. This represents the main contradictory issue in the field of curvature-mediated catalysis. In addition, practical limitations of curvature catalysis include: precise curvature regulation is difficult to achieve on macroscopic catalytic materials, and current high-curvature catalytic interfaces are mostly limited to nanoscale materials at the laboratory scale. Furthermore, the regulatory mechanism of curvature varies considerably across different catalytic reactions, and a unified curvature-design theory has not yet been established, preventing the rational design of catalytic systems.

Beyond the reaction-specific regulatory mechanisms, there exist general cross-catalytic trends in the correlation between curvature and catalytic performance that can be generalized across different catalytic systems. First, high curvature is not always a beneficial structural feature for catalytic reactions: it exerts a prominent promotion effect on reactions that require weakening the excessive adsorption of intermediates (e.g., ORR, CO_2RR) and optimizing the electronic structure of active sites via strain effects, yet it may have a negative impact on reactions that demand strong and stable adsorption of reactants on the catalyst surface (e.g., some selective hydrogenation reactions). Excessively high curvature will introduce severe lattice distortion and reduce the structural stability

of active sites, leading to the decline of catalytic selectivity and long-term cycling performance. Second, an optimal curvature value or curvature range exists for almost all catalytic reactions, which is determined by the intrinsic characteristics of the reaction itself, including the type of active sites, the adsorption strength of key intermediates, and the reaction pathway. For instance, moderate curvature of carbon nano-onion supports can optimize the *OOH adsorption energy of Fe-N_4 sites to the optimal range for ORR, while a slightly higher curvature is required for Zn-N_4 sites to achieve efficient charge injection and selective CO_2RR. This optimal curvature effect is essentially a balance between curvature-induced strain enhancement of catalytic activity and structural stability of the catalyst. Third, the cross-catalytic curvature-performance correlation follows the Sabatier principle in essence: the curvature of the carrier modulates the binding strength between active sites and intermediates by regulating the electronic structure and coordination environment of active sites, and only when the curvature is tuned to match the adsorption energy requirement of the catalytic reaction can the maximum catalytic performance be achieved. These general trends provide a universal theoretical guidance for the rational design of curvature-tailored catalytic carriers across different reaction systems, and the key to practical application is to determine the optimal curvature range for specific catalytic reactions by combining theoretical calculation and experimental verification. In practical catalytic systems, curvature, size and composition exhibit obvious coupling effects, yet curvature regulation can achieve performance enhancement beyond single size or composition optimization. For instance, the high-curvature N-doped carbon-supported C-Fe_1Cr_1NC diatomic nanozyme achieves a 62.0% tumor inhibition rate in vivo, which is significantly higher than the size-optimized non-curvature nanozyme group (44.4%) and the single-component modified Fe_1NC group (≈35%); the high-curvature carbon nano-onion-supported Zn-N_4 single-atom catalyst realizes ＞99% CO_2RR Faraday efficiency, far exceeding the size-reduced Zn-N_4 catalyst (≈85%) and the B-doped planar Zn-N_4 catalyst (≈90%). These results fully verify that curvature regulation, as an independent structural strategy, can synergize with size and composition optimization to achieve a leap in

catalytic performance, and its regulatory value cannot be replaced by simple size or composition adjustment.

3.3 Material assembly application

Curvature carriers, serving as core structural control tools for precisely regulating microscopic assembly processes, have demonstrated value in the fields of superlattice assembly and self-assembly due to their ability to directionally reshape interactions among assembly units. Their key advantage lies in establishing a directional matching mechanism between curvature and interactions by precisely controlling the local curvature of assembly units or carriers. This overcomes bottlenecks in conventional assembly processes, such as poor order, low structural controllability, and kinetic traps.[80,81] Different research teams, guided by this core concept, have conducted innovative explorations in superlattice assembly and self-assembly, proposing distinctive curvature control strategies. These efforts have successfully achieved the controllable preparation of precisely ordered assembly structures and endowed materials with unique functional properties, thereby opening new pathways for the design and synthesis of functional materials with precise structures and tunable performance.[82]

In the field of superlattice assembly, the core value of curvature supports lies in constructing directional interlocking interactions by regulating the local curvature of assembly building blocks, which provides an innovative strategy for breaking through the limitations of traditional assembly driving forces.[83] For superlattice assembly, non-convex dumbbell-shaped nanocrystals (NDs) are used as the core building blocks; by precisely modulating the local curvature of the nanoparticles, directional interaction characteristics analogous to atomic valence bonds are imparted between the particles.[80] Such nanocrystals possess a unique structure with convex heads and concave waists, and their local curvature exhibits inherent self-complementarity, forming a lock and key specific matching mechanism (**Figure 9a-b**). The concave waist of one nanocrystal can precisely interlock with the convex head of another, thus providing a new driving force for the directional assembly of

superlattices. Meanwhile, the introduction of depletion interactions overcomes the kinetic traps of non-convex nanoparticle assembly (**Figure 9c**). Ultimately, long-range ordered interlocking assembly of nanoparticles is achieved, and various complex two-dimensional superlattices, including chiral Kagome lattices, are successfully constructed. This opens up a new pathway for the design and synthesis of superlattice materials with precise structures and tunable properties.

Beyond superlattice assembly, curvature carriers also play a critical regulatory role in the field of self-assembly. By optimizing the curvature environment of carriers or the bending characteristics of building units, they reshape the driving forces of self-assembly and enhance structural order.[84] In the context of self-assembly, research teams have proposed a novel strategy using block copolymers (BCPs) as building units to optimize self-assembly behavior by tuning the core curvature characteristics of microscale photonic crystal (PC) carriers.[85] They designed and fabricated hollow PC microcapsules, leveraging their structural advantage of eliminating the interference caused by the high curvature at the core of solid microspheres (**Figure 9d**). This avoids the periodic structural distortion of BCPs typically induced by the high core curvature in traditional solid PC microspheres. Simultaneously, BCPs achieved long-range ordered concentric lamellar self-assembly within the uniform curvature environment of the microcapsule shell, forming a photonic crystal structure with consistent periodicity. This curvature optimization-ordered assembly matching mechanism not only addresses the challenges of disordered self-assembly structures and poor monochromaticity under solid curvature carriers but also imparts functional properties such as pH responsiveness to the assemblies. This provides a new curvature-driven approach for the directional self-assembly of photonic crystal materials.

A novel self-assembly strategy based on curved perylene diimides ([n]B-PDIs) as curvature carriers was developed. By systematically varying the length of the linear alkyl chains linking the two nitrogen atoms, a gradual transition in molecular bending angle (curvature) was achieved—from planar conformations to highly bent structures with angles up to 45.95° (**Figure 9e-h**). These

curvature carriers leverage curvature-dependent dipole characteristics to reshape the core driving forces of self-assembly, shifting the dominant interaction from dispersion forces in planar molecules to dipole–dipole interactions in bent molecules. This establishes a directional matching mechanism for curvature-regulated forces.[86] Such curvature-mediated "structure–interaction" matching promotes the transition of self-assembled structures from H-aggregates to ordered J-aggregates and further to specific lateral arrangements, while precisely controlling intermolecular binding strength and coupling efficiency. Ultimately, [n]B-PDIs with moderate curvature realized rare symmetry-broken charge separation functions in the crystalline state. This strategy highlights the crucial role of curvature carriers as core regulatory units and provides a new driving force for tailoring self-assembly structures and optimizing the performance of π-functional materials.

In the application of curvature in biomedical materials, the core challenge lies in the contradictory curvature regulation between biocompatibility and functionalization. A moderately low-curvature surface can reduce non-specific cell adhesion and improve the in vivo biocompatibility of biomedical materials. Although high-curvature surfaces can enhance specific interactions between materials and cells (such as promoting stem cell differentiation), they may induce abnormal cell apoptosis or inflammatory responses due to overly complex surface topographical structures. In addition, long-term application limitations of biomedical materials include: the in vivo biodegradation process gradually changes the surface curvature of materials, leading to the decay of their preset functions over time. Meanwhile, the internal curvature of three-dimensional biomedical materials is difficult to accurately characterize and regulate, making it impossible to achieve spatially precise design of material functions.

4. Conclusions and perspectives

This study focuses on the topic of curvature-engineered nanocarriers. By adopting an interdisciplinary research approach, systematic progress has been achieved in four core aspects: the mechanistic understanding of curvature effects, the precise construction of carrier architectures, the

systematic regulation of functional behaviors, and the preliminary validation of practical applications. This study clarifies that curvature is not merely a parameter describing geometric morphology, but also a functional switch that modulates the interfacial properties, electronic structures, and cross-scale behaviors of nanocarriers. The establishment of correlations between curvature and surface stress, charge distribution, as well as motion modes has deepened the understanding of the behavioral mechanisms of nanocarriers in biological, chemical, and physical environments, laying a theoretical foundation for the development of high-performance and intelligent nanosystems.[87]

At the technical level, this study integrates and innovates a variety of curvature-guided synthesis and characterization strategies. Through the development of template-induced synthesis, self-assembly modulation, interfacial buckling, and post-modification etching methods, relatively precise control over the magnitude, distribution, and type of carrier curvature has been realized. Meanwhile, a multi-dimensional characterization system integrating electron microscopy, scattering techniques, mechanical measurements, and computational simulations has been established, which lays the foundation for the quantitative and standardized description of curvature. These methodological advances have transformed curvature from a qualitative concept into a designable, fabricable, and measurable variable in materials science.[88,89] At the application level, this study demonstrates the great potential of curvature modulation in multiple fields. In the biomedical field, curvature design can significantly improve the delivery efficiency and targeting ability of carriers in complex biological microenvironments; in the catalysis field, curvature serves as a new dimension to regulate the electronic states of active sites and optimize reaction pathways; in the field of material assembly, curvature provides a novel driving force for constructing complex superstructures and achieving unusual physicochemical properties. These exploratory applications prove that curvature engineering is an approach to enhance the performance of nanomaterials and break through current technical bottlenecks.[90,91] However, from the perspective of the overall development of this field, three major core common problems remain: First, there is an inherent trade-off between precise control and

scalable preparation of curvature; no fabrication technology has been developed that combines both high controllability and high scalability. Second, the coupling effects between curvature and other material properties (size, charge, composition) are difficult to decouple, and there is a lack of effective methods to independently evaluate the contribution of curvature, leading to contradictions and disputes in some research results. Unlike size and composition regulation, which have been deeply studied for decades and formed mature theoretical systems and industrial preparation technologies, curvature as an independent core design parameter is still in the exploratory stage, with its regulatory mechanism and quantitative evaluation methods to be improved. Nevertheless, existing research has fully proved that curvature breaks through the "passive optimization" limitation of size and composition—which only adjust performance by changing macroscopic scale or chemical properties—and realizes "active programming" of nanocarrier functions by modulating surface stress and electronic structure, making it an important upgrade to the traditional nanomaterial design system. Third, the application of curvature is mostly limited to the laboratory scale; complex environments in vivo or in practical applications significantly alter the performance of curvature, and no curvature‐based design theory suitable for real‐world scenarios has been established. The core development direction of this field in the future should focus on the three key issues: accurate characterization and regulation of curvature, decoupling of coupling effects, and adaptability to practical application scenarios, so as to achieve the leap from fundamental laboratory research to industrialization / clinical application. In particular, developing quantitative decoupling methods for curvature, size and composition is a critical priority: by clarifying the independent contribution and synergistic mechanism of each parameter, we can realize multi-dimensional precise design of nanocarriers, and maximize their performance in practical application scenarios through the integrated regulation of curvature with size optimization and composition modification.

Building on current achievements and looking toward the future, research on curvature nanocarriers will continue to deepen and expand in key directions centered on technical refinement,

mechanism excavation, and practical application.[92,93] In the field of precise curvature regulation technology, the focus will be on developing high-throughput synthesis platforms based on microfluidics and 4D printing, realizing the parallel preparation of curvature-tailored nanocarriers with 10+ different curvature values in a single batch, and reducing the curvature fluctuation range from the current ~10% to <3%; meanwhile, a standardized curvature characterization system combining in-situ EXAFS, cryo-TEM, and geometric modeling will be established to achieve quantitative mapping of local curvature distribution with spatial resolution <5 nm and time resolution <10 ms, enabling dynamic tracking of curvature changes in complex environments such as intracellular endocytosis and catalytic reaction processes.[94,95] In the direction of mechanism-driven performance optimization, efforts will be devoted to the cross-scale structure-activity relationship of curvature, constructing multi-scale simulation models from atomic scale to mesoscale to predict the regulatory effect of curvature on carrier functions—for example, establishing a curvature-endocytosis pathway coupling model in drug delivery to guide the design of carriers with optimal curvature for specific cell types, and developing a curvature-intermediate adsorption energy correlation model in catalysis to realize the rational design of curvature for target reactions such as ORR and CO_2RR, with catalytic activity improved by >50% compared with planar carriers.[96,97] In the construction of biosafety evaluation systems, a curvature-biocompatibility database covering different curvature types (positive/negative/mixed) and material systems (inorganic/polymer/biological) will be established to clarify the influence of curvature on immune response (e.g., complement activation, cytokine secretion) and long-term toxicity (e.g., biodegradation rate, organ accumulation);[98] standardized safety evaluation protocols for curvature carriers will be developed, including in vitro cell viability tests under different curvature conditions and in vivo long-term tracking (≥6 months) of carrier metabolism, providing a scientific basis for clinical translation.[99] In the advancement of industrialization key technologies, low-cost, large-scale synthesis processes for curvature carriers will be developed, such as continuous flow template

synthesis technology and green etching technology, reducing the production cost by >70% compared with laboratory-scale methods; strict quality control standards for curvature parameters will be established, including curvature uniformity, batch stability, and storage stability (≥12 months under standard conditions); pilot applications of curvature carriers will be promoted in fields such as low-dose drug delivery, high-efficiency catalytic hydrogen production, and precision assembly of functional materials, verifying their practical application value in industrial and clinical scenarios.[100,101] In the exploration of interdisciplinary integration, collaboration with biomedicine, chemical engineering, information technology, and other fields will be strengthened to develop innovative application models—for example, combining curvature regulation with targeted ligand modification in precision medicine to develop "curvature-ligand dual-targeted" drug delivery systems for the treatment of refractory tumors such as triple-negative breast cancer, integrating curvature-optimized catalysts into fuel cells and electrolyzers in new energy to improve energy conversion efficiency, and developing curvature-responsive smart materials for self-assembled microdevices and flexible electronics in intelligent manufacturing.[102-104]

In addition, the research on curvature nanocarriers is evolving toward dynamization and extreme scaling, forming two critical cutting-edge directions: First, dynamic/adaptive curvature regulation, driven by 4D printing technologies (e.g., robotic conformal 4D printing, defect-based 4D printing), and classic dynamic polymer insertion methods,[95] enables programmable shape transformation of soft robots and intelligent materials by programming liquid crystal orientation or utilizing residual stress and microdefects,[105,106] This strategy is also verified in the morphogenesis regulation of non-spherical polymersomes (e.g., starfish polymersomes),[107] where local curvature and shape of polymer membranes can be precisely controlled by regulating external stimuli, further expanding the application scenarios of curvature engineering in flexible devices and nanomedicine.[95,107] Second, ultrahigh curvature regimes induce significant quantum confinement effects—polar van der Waals materials rolled into 1D nanoscrolls (near-100% yield via spontaneous

rolling) exhibit broken inversion symmetry and enhanced second harmonic generation (100 times higher than 2D sheets),[105] providing a new pathway for designing quantum nanodevices. These frontier trends will promote the leapfrog development of curvature nanotechnology from fundamental research to functional application innovation.

As a dynamic and emerging field, curvature nanocarriers are at a critical juncture transitioning from fundamental science to functional applications. With further elucidation of their scientific essence and the continuous maturation of engineering technologies, curvature regulation is expected to become one of the core design principles in future nanotechnology. It holds the potential to provide innovative solutions to global challenges in health, energy, and the environment, demonstrating profound and far-reaching scientific and societal value.

Corresponding Authors

*(L.W.) E-mail: inorchemwl@126.com.

*(J.L.) E-mail: jplai@qust.edu.cn.

Conflict of Interest

The authors declare no conflict of interest.

Author contributions

L.W. and J.L. supervised the research. J.L. conceived the research. S.P. collected documents, sorted out materials, and wrote original manuscripts. X.Z., Y.L., and K.S. helped supervision. N.L. Writing-review & editing, Visualization. All authors discussed the results and commented on the manuscript.

Acknowledgment

This work was supported by the National Natural Science Foundation of China (52272222), Taishan Scholar Young Talent Program (tsqn201909114, tsqn201909123), University Youth Innovation Team of Shandong Province (202201010318).

References

[1] C. Wei, R. Joseph Weiblen, C. R. Menyuk, J. Hu, Negative curvature fibers. *Adv. Opt. Photonics* **2017,** *9*, 504-561.

[2] J. Sun, S. Kleuskens, J. Luan, D. Wang, S. Zhang, W. Li, G. Uysal, D. A. Wilson, Morphogenesis of starfish polymersomes. *Nat. Commun.* **2023,** *14*, 3612.

[3] D. Zhang, H. Zhao, X. Wu, Y. Deng, Z. Wang, Y. Han, H. Li, Y. Shi, X. Chen, S. Li, J. Lai, B. Huang, L. Wang, Multi-site electrocatalysts boost pH-universal nitrogen reduction by high-entropy alloys. *Adv. Funct. Mater.* **2021,** *31*, 2006939.

[4] W. Yu, Y. Zhang, Y. Qin, D. Zhang, K. Liu, G. A. Bagliuk, J. Lai, L. Wang, High-density frustrated lewis pair for high-performance hydrogen evolution. *Adv. Energy Mater.* **2023,** *13*, 2203136.

[5] J.-N. Liu, C.-X. Zhao, J. Wang, X.-Q. Fang, C.-X. Bi, B.-Q. Li, Q. Zhang, A data-driven bifunctional oxygen electrocatalyst with a record-breaking $\Delta E = 0.57$ *V* for ampere-hour-scale zinc-air batteries. *Joule* **2024,** *8*, 1804-1819.

[6] Y. Hao, Y. Li, J. Wu, L. Meng, J. Wang, C. Jia, T. Liu, X. Yang, Z.-P. Liu, M. Gong, Recognition of surface oxygen Intermediates on NiFe oxyhydroxide oxygen-evolving catalysts by homogeneous oxidation reactivity. *J. Am. Chem. Soc.* **2021,** *143*, 1493-1502.

[7] J. Su, C. B. Musgrave, Y. Song, L. Huang, Y. Liu, G. Li, Y. Xin, P. Xiong, M. M.-J. Li, H. Wu, M. Zhu, H. M. Chen, J. Zhang, H. Shen, B. Z. Tang, M. Robert, W. A. Goddard, R. Ye, Strain enhances the activity of molecular electrocatalysts via carbon nanotube supports. *Nat. Catal.* **2023,** *6*, 818-828.

[8] Y.-W. Yin, Y.-Q. Ma, H.-M. Ding, Effect of nanoparticle curvature on its interaction with serum proteins. *Langmuir.* **2024,** *40*, 15205-15213.

[9] Z. Hao, J. Chen, D. Zhang, L. Zheng, Y. Li, Z. Yin, G. He, L. Jiao, Z. Wen, X.-J. Lv, Coupling effects of Zn single atom and high curvature supports for improved performance of CO_2 reduction. *Sci. Bull.* **2021,** *66*, 1649-1658.

[10] P.-L. Latreille, J.-M. Rabanel, M. Le Goas, S. Salimi, J. Arlt, S. A. Patten, C. Ramassamy, P. Hildgen, V. A. Martinez, X. Banquy, In Situ Characterization of the Protein Corona of Nanoparticles In Vitro and In Vivo. *Adv. Mater.* **2022,** *34*, 2203354.

[11] X. Shang, H. Chen, V. Castagnola, K. Liu, L. Boselli, V. Petseva, L. Yu, L. Xiao, M. He, F. Wang, K. A. Dawson, J. Fan, Unusual zymogen activation patterns in the protein corona of Ca-zeolites. *Nat. Catal.* **2021,** *4*, 607-614.

[12] P. Strzyz, Curvature-mediated endocytosis. *Nat. Rev. Mol. Cell Biol.* **2022,** *23*, 447-447.

[13] P. Pámies, Sorted by curvature. *Nat. Mater.* **2015,** *14*, 1186-1186.

[14] H. Wang, H. Xu, F. Yang, Y. Qing, F. Chu, Y. Wu, S. Ye, F. Xiong, Enhancing Field Effects of Single-Atom Ru/Lignin Carbon Nanoreactors for Electrocatalytic Hydrogen Evolution by Continuous Heterogeneous Curvature. *Adv. Mater.* **2026,** *38*, e15230.

[15] Q. Wang, L. Lyu, N. Han, B. Chu, C. Shang, Z. Wang, H. Pan, D. Lee, W. Zhang, J. Zhang, Z. Li, W. Huang, Y.-M. Kang, Dual modulation of coordination asymmetry and curvature unlocks record-level Zn–air battery performance with Fe–N–C single-atom catalysts. *Energy Environ. Sci.* **2025,** *18*, 10390-10402.

[16] J. H. Seol, I. Jo, A. L. Moore, L. Lindsay, Z. H. Aitken, M. T. Pettes, X. Li, Z. Yao, R. Huang, D. Broido, N. Mingo, R. S. Ruoff, L. Shi, Two-dimensional phonon transport in supported graphene. *Science* **2010,** *328*, 213-216.

[17] X. Li, L. Matino, W. Zhang, L. Klausen, A. F. McGuire, C. Lubrano, W. Zhao, F. Santoro, B. Cui, A nanostructure platform for live-cell manipulation of membrane curvature. *Nat. Protoc.* **2019,** *14*, 1772-1802.

[18] H. Li, J. Lai, Z. Li, L. Wang, Multi-sites electrocatalysis in high-entropy alloys. *Adv. Funct. Mater.* **2021,** *31*, 2106715.

[19] W. Liu, G. Long, Z. Xiang, T. Ren, J. Piao, K. Wan, Z. Fu, Z. Liang, Extremely active and robust Ir−Mn dual-atom electrocatalyst for oxygen evolution reaction by oxygen-oxygen radical coupling mechanism. *Angew. Chem. Int. Ed.* **2024,** *63*, e202411014.

[20] F. Lorenzutti, R. R. Seemakurthi, E. F. Johnson, S. Morandi, P. Nikačević, N. López, S. Haussener, Microenvironment effects in electrochemical CO_2 reduction from first-principles multiscale modelling. *Nat. Catal.* **2025,** *8*, 905-918.

[21] X. Zhang, J. Lu, J. Liu, M. Sun, G. Zhang, S. Kong, M. Zhang, J. Wang, Z. Li, X. Shi, Curvature geometry–spin electronics–catalytic dynamics coupling in emerging catalytic engineering. *Chem. Soc. Rev.* **2026,** *55*, 2691-2730.

[22] W. He, J. Yu, X. Zhang, Y. Zhou, Y. Yao, C. Ma, C. Yin, W. Yan, Y. Liu, C. Lu, X. Li, Growth mechanism of graphite-carbon encapsulated nickel catalysts and curvature effect of carbon layer on the performance of catalytic hydrogenation. *Appl. Catal. B Environ.* **2023,** *331*, 122738.

[23] Z. Wang, Z. Yang, Z. C. Kadirova, M. Guo, R. Fang, J. He, Y. Yan, J. Ran, Photothermal functional material and structure for photothermal catalytic CO_2 reduction: Recent advance, application and prospect. *Coord. Chem. Rev.* **2022,** *473*, 214794.

[24] W. J. Stark, P. R. Stoessel, W. Wohlleben, A. Hafner, Industrial applications of nanoparticles. *Chem. Soc. Rev.* **2015,** *44*, 5793-5805.

[25] Z. Yan, Z. Wu, S. Li, X. Zhang, X. Yi, T. Yue, Curvature-mediated cooperative wrapping of multiple nanoparticles at the same and opposite membrane sides. *Nanoscale* **2019,** *11*, 19751-19762.

[26] F. Bonazzi, T. R. Weikl, Membrane-mediated interactions between arc-shaped particles strongly depend on membrane curvature. *Nanoscale* **2025,** *17*, 6841-6853.

[27] T. Chen, Y. Zhang, X. Li, C. Li, T. Lu, S. Xiao, H. Liang, Curvature-mediated pair interactions of soft nanoparticles adhered to a cell membrane. *J. Chem. Theory Comput.* **2021,** *17*, 7850-7861.

[28] R. J. Nap, E. Gonzalez Solveyra, I. Szleifer, The interplay of nanointerface curvature and calcium binding in weak polyelectrolyte-coated nanoparticles. *Biomater. Sci.* **2018,** *6*, 1048-1058.

[29] W. Sun, Y. Xu, Y. Zhou, Z. Zeng, L. Wang, J. Ouyang, Topographic scanning electronic microscopy reveals the 3D surface structure of materials. *Adv. Funct. Mater.* **2025,** *35*, 2420372.

[30] S. Hwang, X. Chen, G. Zhou, D. Su, In situ transmission electron microscopy on energy-related catalysis. *Adv. Energy Mater.* **2020,** *10*, 1902105.

[31] A. Singh, Automated atomic modeling in cryo-EM maps. *Nature Methods* **2024,** *21*, 749-749.

[32] M. Kagias, Z. Wang, M. E. Birkbak, E. Lauridsen, M. Abis, G. Lovric, K. Jefimovs, M. Stampanoni, Diffractive small angle X-ray scattering imaging for anisotropic structures. *Nat. Commun.* **2019,** *10*, 5130.

[33] G. R. Heath, E. Kots, J. L. Robertson, S. Lansky, G. Khelashvili, H. Weinstein, S. Scheuring, Localization atomic force microscopy. *Nature* **2021,** *594*, 385-390.

[34] L. Gross, B. Schuler, N. Pavliček, S. Fatayer, Z. Majzik, N. Moll, D. Peña, G. Meyer, Atomic force microscopy for molecular structure elucidation. *Angew. Chem. Int. Ed.* **2018,** *57*, 3888-3908.

[35] J. Schindelin, I. Arganda-Carreras, E. Frise, V. Kaynig, M. Longair, T. Pietzsch, S. Preibisch, C. Rueden, S. Saalfeld, B. Schmid, J.-Y. Tinevez, D. J. White, V. Hartenstein, K. Eliceiri, P. Tomancak, A. Cardona, Fiji: an open-source platform for biological-image analysis. *Nature Methods* **2012,** *9*, 676-682.

[36] X. Wu, X. Tian, W. Zhang, X. Peng, S. Zhou, P. J. S. Buenconsejo, Y. Li, S. Xiao, J. Tao, M. Zhang, H. Yuan, Solution-processable MOF-on-MOF system constructed via template-assisted growth for ultratrace H2S detection. *Angew. Chem. Int. Ed.* **2024,** *63*, e202410411.

[37] J. Huang, Y. Shi, J. Xu, J. Zheng, F. Zhu, X. Liu, G. Ouyang, Hollow covalent organic framework with “shell-confined” environment for the effective removal of anionic per- and polyfluoroalkyl substances. *Adv. Funct. Mater.* **2022,** *32*, 2203171.

[38] P. Liu, X. Zhang, J. Fei, Y. Shi, J. Zhu, D. Zhang, L. Zhao, L. Wang, J. Lai, Frank partial dislocations in coplanar Ir/C ultrathin aanosheets boost hydrogen evolution reaction. *Adv. Mater.* **2024,** *36*, 2310591.

[39] H. Li, Y. Han, H. Zhao, W. Qi, D. Zhang, Y. Yu, W. Cai, S. Li, J. Lai, B. Huang, L. Wang, Fast site-to-site electron transfer of high-entropy alloy nanocatalyst driving redox electrocatalysis. *Nat. Commun.* **2020,** *11*, 5437.

[40] D. Zhang, Y. Shi, H. Zhao, W. Qi, X. Chen, T. Zhan, S. Li, B. Yang, M. Sun, J. Lai, B. Huang, L. Wang, The facile oil-phase synthesis of a multi-site synergistic high-entropy alloy to promote the alkaline hydrogen evolution reaction. *J. Mater. Chem. A* **2021,** *9*, 889-893.

[41] D. Zhang, H. Zhao, B. Huang, B. Li, H. Li, Y. Han, Z. Wang, X. Wu, Y. Pan, Y. Sun, X. Sun, J. Lai, L. Wang, Advanced ultrathin RuPdM (M = Ni, Co, Fe) nanosheets electrocatalyst boosts hydrogen evolution. *ACS Cent. Sci.* **2019,** *5*, 1991-1997.

[42] Y. Chen, M. Tan, R. Yang, C. K. W. Lee, H. Zhong, Y. Xu, Y. Huang, M. Tang, M. G. Li, Laser-guided self-assembly of thin films into micro-rolls. *Adv. Funct. Mater.* **2024,** *34*, 2400090.

[43] G. M. Whitesides, B. Grzybowski, Self-assembly at all scales. *Science* **2002,** *295*, 2418-2421.

[44] H. Luan, Q. Zhang, T.-L. Liu, X. Wang, S. Zhao, H. Wang, S. Yao, Y. Xue, J. W. Kwak, W. Bai, Y. Xu, M. Han, K. Li, Z. Li, X. Ni, J. Ye, D. Choi, Q. Yang, J.-H. Kim, S. Li, S. Chen, C. Wu, D. Lu, J.-K. Chang, Z. Xie, Y. Huang, J. A. Rogers, Complex 3D microfluidic architectures formed by mechanically guided compressive buckling. *Sci. Adv.* **2021,** *7*, eabj3686.

[45] A. Djellouli, B. Van Raemdonck, Y. Wang, Y. Yang, A. Caillaud, D. Weitz, S. Rubinstein, B. Gorissen, K. Bertoldi, Shell buckling for programmable metafluids. *Nature* **2024,** *628*, 545-550.

[46] X. Tian, R. Liu, W. Wang, Q. Yang, Z. Huang, Y. Yang, J. Han, T. Dong, Y. Du, J. Lai, H. Li, L. Wang, 3D ordered macroporous superstructures of high entropy hydroxide with strong orbital coupling enhancing water/seawater oxidation. *Adv. Mater.* **2025,** *37*, e06068.

[47] M. He, P. Wang, P. Xiao, X. Jia, J. Luo, B. Jiang, Hollow silica nanospheres synthesized by one-step etching method to construct optical coatings with controllable ultra-low refractive index. *COLLOID SURFACE A* **2023,** *670*, 131433.

[48] L. Chen, X. Dai, W. Feng, Y. Chen, Biomedical applications of MXenes: From nanomedicine to biomaterials. *Accounts of Materials Research* **2022,** *3*, 785-798.

[49] H. Tang, Y. Zheng, Y. Chen, Materials chemistry of nanoultrasonic biomedicine. *Adv. Mater.* **2017,** *29*, 1604105.

[50] V. Francia, C. Reker-Smit, A. Salvati, Mechanisms of uptake and membrane curvature generation for the internalization of silica nanoparticles by cells. *Nano Letters* **2022,** *22*, 3118-3124.

[51] W. Jia, Y. Wang, R. Liu, X. Yu, H. Gao, Shape Transformable Strategies for Drug Delivery. *Adv. Funct. Mater.* **2021,** *31*, 2009765.

[52] Z. Li, Y. Zhang, L. Wu, W. Yu, T. R. Wilks, A. P. Dove, H. M. Ding, R. K. O'Reilly, G. Chen, M. Jiang, Glyco-Platelets with Controlled Morphologies via Crystallization-Driven Self-Assembly and Their Shape-Dependent Interplay with Macrophages. *ACS macro letters* **2019,** *8*, 596-602.

[53] H. Y. Zhao, Y. Q. Chen, X. Y. Luo, M. J. Cai, J. Y. Li, X. Y. Lin, H. Zhang, H. M. Ding, G. L. Jiang, Y. Hu, Ligand Phase Separation-Promoted, "Squeezing-Out" Mode Explaining the Mechanism and Implications of Neutral Nanoparticles That Escaped from Lysosomes. *ACS Nano* **2024,** *18*, 2162-2183.

[54] Q. Chen, Loading α-helical peptide drugs onto nanotubes: Influence of surface curvature and van der Waals/electrostatic interactions. *Appl. Surf. Sci.* **2025,** *688*, 162467.

[55] Y. W. Yin, Y. Q. Ma, H. M. Ding, Effect of Nanoparticle Curvature on Its Interaction with Serum Proteins. *Langmuir* **2024,** *40*, 15205-15213.

[56] X. Jiang, S. Xu, Y. Miao, K. Huang, B. Wang, B. Ding, Z. Zhang, Z. Zhao, X. Zhang, X. Shi, M. Yu, F. Tian, Y. Gan, Curvature-mediated rapid extravasation and penetration of nanoparticles against

interstitial fluid pressure for improved drug delivery. *Proceedings of the National Academy of Sciences* **2024,** *121*, e2319880121.

[57]P. K. Pandey, P. P. Singh, S. Khatua, R. Ranganathan, A. Mishra, In Vitro and In-Silico Assessment of Gaussian Curvature-driven Internalization Kinetics of Nanoparticles. *ACS Appl. Mater. Interfaces* **2025,** *17*, 663-674.

[58]C. Jiang, S. Wang, S. Li, G. Wang, J. Guo, Q. Hu, Z. Wang, L. Li, Z. Chen, Curved carbon-supported dual-atom nanozyme with ascorbic acid oxidase activity for cascade tumor catalytic therapy. *ACS nano* **2025,** *19*, 38053-38066.

[59]B. Diloknawarit, E. N. Schaumann, T. W. Odom, High-curvature features on branched nanoconstructs circumvent protein corona interference. *ACS Appl. Mater. Interfaces* **2025,** *17*, 15187-15195.

[60]X. Hu, X. Chen, X. Shi, J. Gao, Z. Ao, N. Li, J. Yuan, X. Fang, Z. Qiu, Z. Zhou, Y. Liao, D. Han, Bionanoparticle-based delivery in antihypertensive vaccine mediates DC activation through lipid-raft reorganization. *Adv. Funct. Mater.* **2020,** *30*, 2000346.

[61]L. Schoonen, J. C. M. van Hest, Functionalization of protein-based nanocages for drug delivery applications. *Nanoscale* **2014,** *6*, 7124-7141.

[62]C. Zhu, D. Wang, L. Zeng, G. Feng, Y. Liang, W. Zheng, W. Lin, X. Peng, Z. Liu, X. Sang, B. Yang, Z. Li, Q. Zhang, L. Lei, Y. Hou, Engineering the coordination environment of metal centers for selective and high-current CO2 electromethanation. *J. Am. Chem. Soc.* **2025,** *147*, 26185-26194.

[63]G. Xu, J. Li, Y. Zeng, Z. Shi, W. Qi, K. Li, M. Xiao, C. Liu, W. Xing, J. Zhu, Synergy of Ni single atom and RuNi alloy nanocluster enables boosted hydrogen evolution at industrial current densities. *Energy Environ. Sci.* **2025,** *18*, 6273-6282.

[64]X. Wu, Z. Wang, D. Zhang, Y. Qin, M. Wang, Y. Han, T. Zhan, B. Yang, S. Li, J. Lai, L. Wang, Solvent-free microwave synthesis of ultra-small Ru-Mo_2C@CNT with strong metal-support interaction for industrial hydrogen evolution. *Nat. Commun.* **2021,** *12*, 4018.

[65] L. Zhao, Z. Lv, Y. Shi, S. Zhou, Y. Liu, J. Han, Q. Zhang, J. Lai, L. Wang, Correction: Simultaneous generation of furfuryl alcohol, formate, and H_2 by co-electrolysis of furfural and HCHO over bifunctional CuAg bimetallic electrocatalysts at ultra-low voltage. *Energy Environ. Sci.* **2024,** *17*, 1291-1291.

[66] Y. Yu, Y. Sun, J. Han, Y. Guan, H. Li, L. Wang, J. Lai, Achieving efficient urea electrosynthesis through improving the coverage of a crucial intermediate across a broad range of nitrate concentrations. *Energy Environ. Sci.* **2024,** *17*, 5183-5190.

[67] S. Zhou, Y. Shi, Y. Dai, T. Zhan, J. Lai, L. Wang, Continuous-flow electrosynthesis of urea and oxalic acid by CO_2-nitrate reduction and glycerol oxidation. *Chin. J. Catal.* **2024,** *63*, 270-281.

[68] Q. Wang, L. Lyu, X. Hu, W. Fan, C. Shang, Q. Huang, Z. Li, Z. Zhou, Y.-M. Kang, Tailoring the surface curvature of the supporting carbon to tune the d-band center of Fe-N-C single-atom catalysts for Zinc-Urea-Air batteries. *Angew. Chem. Int. Ed.* **2025,** *64*, e202422920.

[69] W. Cao, M. Figueras-Valls, F. Viñes, F. Illas, Understanding the curvature effect on the structure and bonding of MoCy nanoparticles on carbon supports. *ACS Appl. Mater. Interfaces* **2025,** *17*, 7098-7108.

[70] Y. Yu, Z. Lv, Z. Liu, Y. Sun, Y. Wei, X. Ji, Y. Li, H. Li, L. Wang, J. Lai, Activation of Ga liquid catalyst with continuously exposed active sites for electrocatalytic C−N coupling. *Angew. Chem. Int. Ed.* **2024,** *63*, e202402236.

[71] D. Liu, X. Li, S. Chen, H. Yan, C. Wang, C. Wu, Y. A. Haleem, S. Duan, J. Lu, B. Ge, P. M. Ajayan, Y. Luo, J. Jiang, L. Song, Atomically dispersed platinum supported on curved carbon supports for efficient electrocatalytic hydrogen evolution. *Nat. Energy* **2019,** *4*, 512-518.

[72] Y. Yu, J. Han, H. Li, H. Diao, Y. Shi, G. Jin, H. Li, G. A. Bagliuk, L. Wang, J. Lai, CuPt alloy enabling the tandem catalysis for reduction of HCOOH and NO_3^- to urea at high current density. *Adv. Mater.* **2025,** *37*, 2419738.

[73] Y. Mao, W. Ma, W. Zuo, H. Sun, Y. Tian, J. Zhang, L. Li, Breaking planar confinement: Tailoring the curvature of nanoconfined catalysts to activate PMS for efficient $^1O_2$ generation. *Appl. Catal. B Environ* **2026,** *385*, 126266.

[74] H.-F. Wang, L.-N. Song, S. Wang, S.-J. Ding, J.-J. Xu, Local electric field-driven reaction pathway regulation via Ru single atoms on highly curved carbon sphere for stable Li–O_2 batteries. *Angew. Chem. Int. Ed.* **2025,** *n/a*, e21423.

[75] Y. Zhao, J. Wan, C. Ling, Y. Wang, H. He, N. Yang, R. Wen, Q. Zhang, L. Gu, B. Yang, Z. Xiang, C. Chen, J. Wang, X. Wang, Y. Wang, H. Tao, X. Li, B. Liu, S. Zhang, D. Wang, Acidic oxygen reduction by single-atom Fe catalysts on curved supports. *Nature* **2025,** *644*, 668-675.

[76] B. Wang, M. Wang, Z. Fan, C. Ma, S. Xi, L. Y. Chang, M. Zhang, N. Ling, Z. Mi, S. Chen, W. R. Leow, J. Zhang, D. Wang, Y. Lum, Nanocurvature-induced field effects enable control over the activity of single-atom electrocatalysts. *Nat. Commun.* **2024,** *15*, 1719.

[77] Y. Shi, L. Song, Y. Liu, T. Wang, C. Li, J. Lai, L. Wang, Dual cocatalytic sites synergize NiFe layered double hydroxide to boost oxygen evolution reaction in anion exchange membrane water electrolyzer. *Adv. Energy Mater.* **2024,** *14*, 2402046.

[78] L. Li, Y. Liu, X. Zhang, M. Humayun, H. Yang, J. Zeng, H. A. Younus, Y. Pang, D. Wang, R. Snyders, C. Wang, Curvature strain-induced electron spin leveraging in d orbitals toward oxygen reduction for Zn–Air batteries. *Nano Letters* **2025,** *25*, 16459-16467.

[79] Y. Liu, L. Xing, Y. Liu, D. Lian, M. Chen, W. Zhang, K. Wu, H. Zhu, Z. Sun, W. Chen, P. Wu, D. Wang, Y. Ji, Strain regulation of bond length in single Ru sites via curving support surface for enhanced hydrogen evolution reaction. *Appl. Catal. B Environ* **2024,** *353*, 124088.

[80] S. Wan, X. Xia, Y. Gao, H. Zhang, Z. Zhang, F. Wu, X. Wu, D. Yang, T. Li, J. Li, R. Ni, A. Dong, Curvature-guided depletion stabilizes Kagome superlattices of nanocrystals. *Science* **2025,** *387*, 978-984.

[81]C. T. Presley, F. Guevara Vasquez, B. Raeymaekers, Multi-frequency ultrasound directed self-assembly. *Adv. Funct. Mater.* **2024,** *34*, 2400193.

[82]H. Li, M. Sun, Y. Pan, J. Xiong, H. Du, Y. Yu, S. Feng, Z. Li, J. Lai, B. Huang, L. Wang, The self-complementary effect through strong orbital coupling in ultrathin high-entropy alloy nanowires boosting pH-universal multifunctional electrocatalysis. *Appl. Catal. B Environ.* **2022,** *312*, 121431.

[83]A. Neophytou, F. Sciortino, J. Russo, Designing the self-assembly of disordered materials via color frustration. *Adv. Mater.* **2025,** *37*, 2502136.

[84]J. Nie, J. Zhao, L. Li, T. Zhou, G. Guerin, Crystallization-driven self-assembly-substrated-polymerization-induced self-assembly (CDSA-s-PISA). Toward the next generation of supercarriers. *Angew. Chem. Int. Ed.* **2025,** *64*, e202511515.

[85]Y. Yang, Y. Chen, Z. Hou, F. Li, M. Xu, Y. Liu, D. Tian, L. Zhang, J. Xu, J. Zhu, Responsive photonic crystal microcapsules of block copolymers with enhanced monochromaticity. *ACS nano* **2020,** *14*, 16057-16064.

[86]R. Wang, B. Qian, Y. Xu, D. Zhao, Q. Chen, Y. Wei, C. Zhang, W. Liang, Y.-B. Jiang, H.-J. Zhang, J. Lin, Self-assembled bent perylenediimides. *Angew. Chem. Int. Ed.* **2025,** *64*, e202421871.

[87]D. Zhang, Y. Shi, X. Chen, J. Lai, B. Huang, L. Wang, High-entropy alloy metallene for highly efficient overall water splitting in acidic media. *Chin. J. Catal.* **2023,** *45*, 174-183.

[88]E. Vargo, J. C. Dahl, K. M. Evans, T. Khan, P. Alivisatos, T. Xu, Using machine learning to predict and understand complex self-assembly behaviors of a multicomponent nanocomposite. *Adv. Mater.* **2022,** *34*, 2203168.

[89]M. Kløve, S. Sommer, B. B. Iversen, B. Hammer, W. Dononelli, A machine-learning-based approach for solving atomic structures of nanomaterials combining pair distribution functions with density functional theory. *Adv. Mater.* **2023,** *35*, 2208220.

[90]Y. Li, S. Kumar, G. Yang, J. Lu, Y. Yao, K. Kang, Z. W. Seh, The contrast between monovalent and multivalent metal battery anodes. *Science* **2025,** *389*, eadl5482.

[91] S. Zhang, L. Zhang, Z.-S. Wu, Solid Lithiation and Exfoliation for Scalable Synthesis of Two-Dimensional Nanosheets toward Industrialization. *ACS Nano* **2024,** *18*, 24617-24621.

[92] H. T. Vengateswaran, M. Habeeb, R. Ahmed, H. W. You, S. T. Kumbhar, K. N. V. Chenchu Lakshmi, P. L. Gorde, Integrating artificial intelligence for design, optimization and pharmacokinetic prediction in nanoparticle based drug delivery. *J. Drug Delivery Sci. Technol.* **2026,** *115*, 107805.

[93] M. A. Mohd Adnan, M. A. Mat Norman, M. F. Majnis, H. A. Tajarudin, N. Muhd Julkapli, Predictive modelling of antibacterial efficacy in TiO_2/ZnO/CS nanocomposites using artificial neural networks. *Int. J. Biol. Macromol.* **2026,** *348*, 150857.

[94] M. A. H. Khan, A. Motayed, M. V. Rao, Identification and quantification of gases and their mixtures using GaN sensor array and artificial neural network. *Meas. Sci. Technol.* **2021,** *32*, 055111.

[95] J. Sun, S. J. Rijpkema, J. Luan, S. Zhang, D. A. Wilson, Generating biomembrane-like local curvature in polymersomes via dynamic polymer insertion. *Nat. Commun.* **2021,** *12*, 2235.

[96] X. Dai, Y. Chen, Computational biomaterials: Computational simulations for biomedicine. *Adv. Mater.* **2023,** *35*, 2204798.

[97] Z. Lv, S. Zhou, L. Zhao, Z. Liu, J. Liu, W. Xu, L. Wang, J. Lai, Coactivation of multiphase reactants for the electrosynthesis of urea. *Adv. Energy Mater.* **2023,** *13*, 2300946.

[98] G. Ma, H. Al-Mahayni, N. Jiang, D. Song, B. Qiao, Z. Xu, A. Seifitokaldani, S. Zhao, Z. Liang, Electrokinetic analyses uncover the rate-determining step of biomass-derived monosaccharide electroreduction on Copper. *Angew. Chem. Int. Ed.* **2024,** *63*, e202401602.

[99] Y. Cao, P. Rewatkar, R. Wang, S. Z. Hasnain, A. Popat, T. Kumeria, Nanocarriers for oral delivery of biologics: small carriers for big payloads. *Trends Pharmacol. Sci.* **2021,** *42*, 957-972.

[100] J. Zhou, A. I. Chizhik, S. Chu, D. Jin, Single-particle spectroscopy for functional nanomaterials. *Nature* **2020,** *579*, 41-50.

[101] K. R. Ryan, M. P. Down, N. J. Hurst, E. M. Keefe, C. E. Banks, Additive manufacturing (3D printing) of electrically conductive polymers and polymer nanocomposites and their applications. *eScience* **2022,** *2*, 365-381.

[102] M.-C. Li, X. Liu, K. Lv, J. Sun, C. Dai, B. Liao, C. Liu, C. Mei, Q. Wu, M. Hubbe, Cellulose nanomaterials in oil and gas industry: Current status and future perspectives. *Prog. Mater Sci.* **2023,** *139*, 101187.

[103] Z. Pei, H. Lei, L. Cheng, Bioactive inorganic nanomaterials for cancer theranostics. *Chem. Soc. Rev.* **2023,** *52*, 2031-2081.

[104] Q. Zhang, Z. Fu, Interdisciplinary Materials: Interdisciplinary and frontier researches between materials science and other disciplines. *Interdisc. Mater.* **2022,** *1*, 5-5.

[105] Z. Zhang, Y. Zhang, K. Lu, J. J. Zhang, N. Zhang, R. Feng, H. Ye, X. Zhou, L. Li, D. Wan, J. Lu, Z. Ni, J. Wang, Q. Chen, J. Lu, Z. Li, Near-100% spontaneous rolling up of polar van der Waals materials. *Nat Mater* **2025,** *24*, 1716-1725.

[106] V. Moosabeiki, E. Yarali, A. Ghalayaniesfahani, S. J. P. Callens, T. van Manen, A. Accardo, S. Ghodrat, J. Bico, M. Habibi, M. J. Mirzaali, A. A. Zadpoor, Curvature tuning through defect-based 4D printing. *Communications Materials* **2024,** *5*, 10.

[107] J. Sun, S. Kleuskens, J. Luan, D. Wang, S. Zhang, W. Li, G. Uysal, D. A. Wilson, Morphogenesis of starfish polymersomes. *Nat. Commun.* **2023,** *14*, 3612.

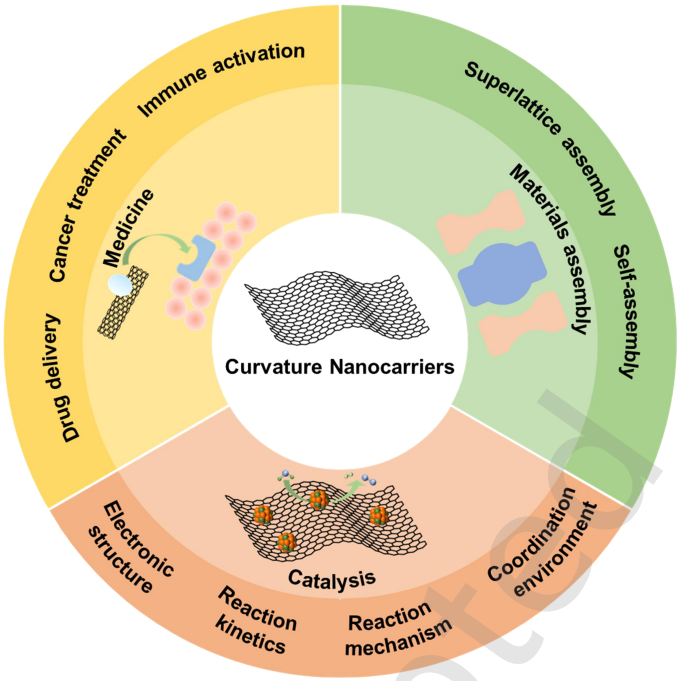

Figure 1. Application scenarios of curvature nanocarriers.

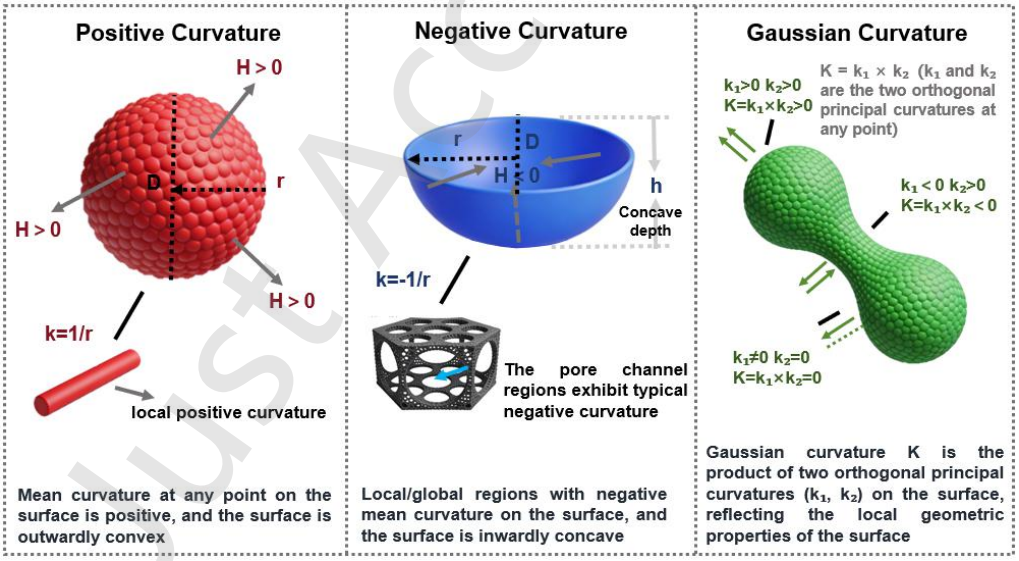

Figure 2. Schematic illustration of positive, negative and gaussian curvature on nanocarriers.

Characterization techniques	Spatial resolution	Core Advantages	Core disadvantages	Applicable sample types
Transmission Electron Microscope (TEM)	0.1 nm	curvature visualization, high precision	samples need to be dry and prone to morphological distortion	inorganic/rigid polymer curvature carriers
Atomic Force Microscope (AFM)	0.01 nm	in-situ characterization, suitable for soft materials	slow testing speed and small field of view	2D materials / biomembrane curvature structures
Cryo-electron microscopy (Cryo-TEM)	0.1 nm	in-situ characterization, no sample distortion	expensive equipment and high testing cost	soft polymer vesicles / protein-based curvature carriers
Fluorescence imaging method	100 nm	in vivo, in-situ real-time monitoring	low resolution, cannot quantify curvature	curvature nanocarriers for in vivo delivery

Table 1. Comparative analysis of curvature characterization techniques.

Synthesis Methods	Achievable curvature range	Core Advantages	Core disadvantages	Scalability	Typical application scenarios
Template method	low to medium curvature (10~100 nm)	controllable morphology and high repeatability	template removal is tedious and easy to introduce impurities	medium	spherical / rod-shaped curvature nanoparticles
Self-assembly method	low to ultra-high curvature (<5 nm~μm)	simple operation, no template required	poor curvature uniformity and difficult to precisely control	high	polymer vesicles / 2D material nanoscrolls
Microfluidic preparation method	medium to high curvature (5~50 nm)	precise curvature control and uniform particle size	high equipment requirements and complicated process	low	customized non-spherical curvature carriers
Defect modulation method (4D printing)	dynamically tunable curvature (tunable range > 50 nm)	dynamic adaptability and shape programmability	high cost and limited applicable materials	low	soft robots / intelligent adaptive carriers

Table 2. Comparative analysis of main synthesis methods for curvature nanocarriers.

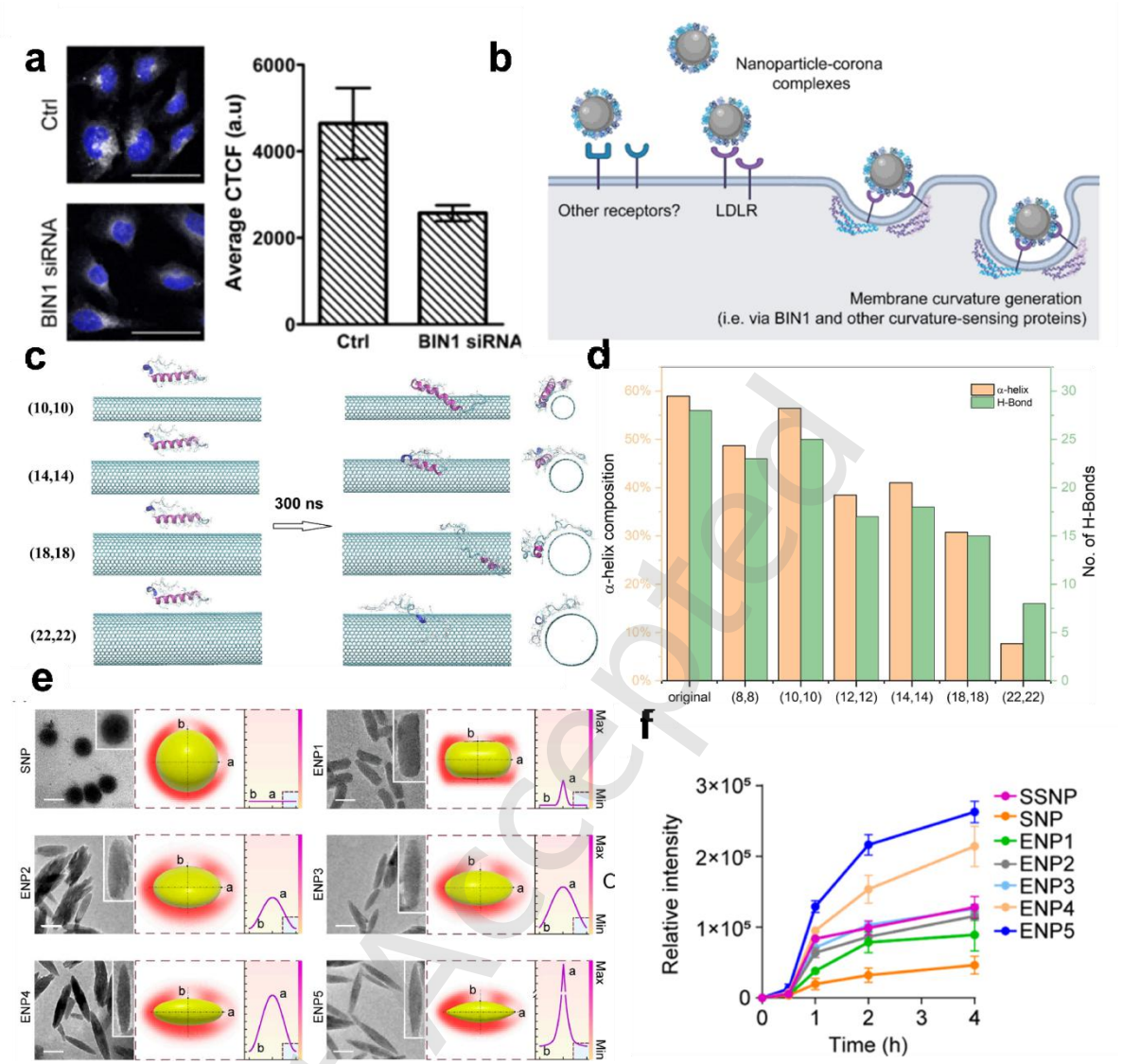

Figure 3. (a) Confocal fluorescence images and corresponding intensity quantification of HeLa cells silenced for BIN1 and exposed for 14 h to 100 µg/mL corona-coated SiO_2 nanoparticles. The results are the average corrected total cell fluorescence obtained from at least 4 images for each condition and confirm strong uptake reduction in BIN1 silenced cells. Scale bars 50 µm. Blue: DAPI for nuclei. (b) Proposed alternative mechanism of membrane curvature generation and nanoparticle uptake. The nanoparticle-corona complexes interact with the LDLR and possibly other receptors and induce membrane bending. (c) Initial and final snapshots from the four 300-ns simulations of EXN interacting with (10,10), (14,14), (18,18), and (22,22) CNTs. (d) α-helix composition and number of internal hydrogen bonds in EXN at the final frame (300 ns) of simulations with CNTs of varying diameters. (e) Characterization of NPs of different curvatures. (Scale bar, 100 nm.) (f) The cumulative extravasation percentage obtained by the in vitro modeling of extravasation at distinct time points.

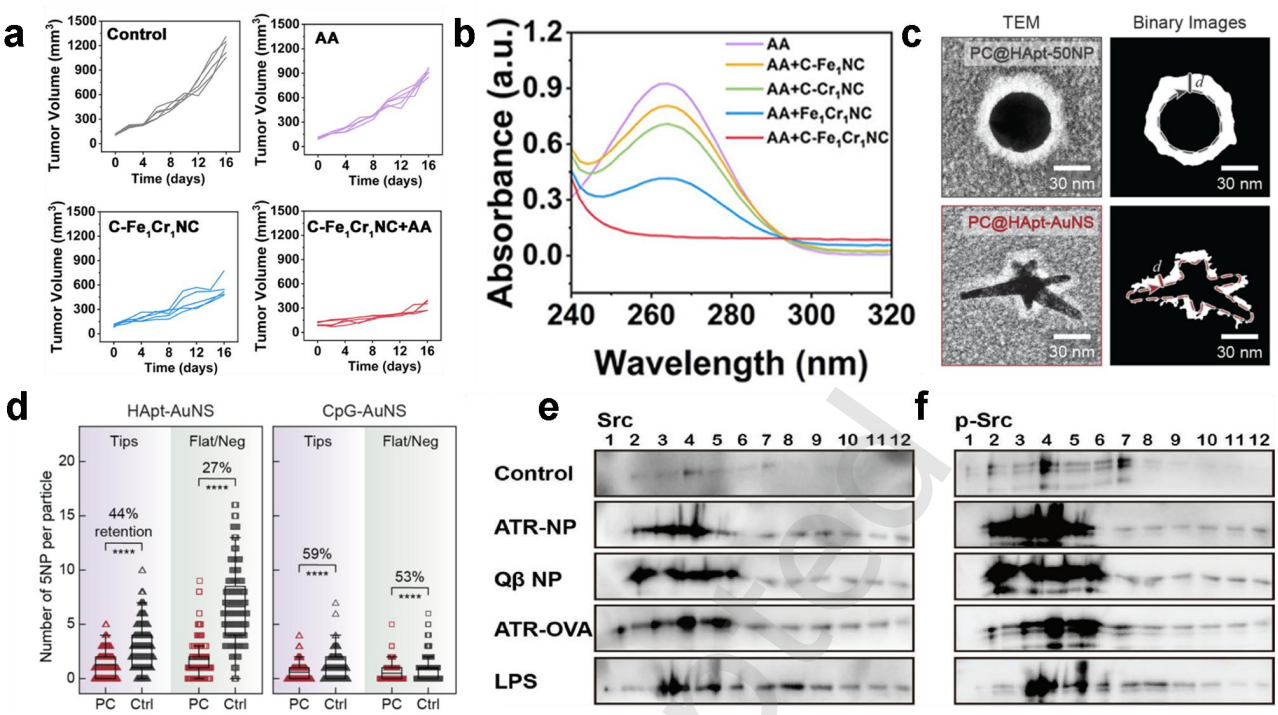

Figure 4. (a) Individual tumor growth curves of mice following various treatments. (b) UV-vis spectra of AA oxidation catalyzed by C-Fe_1Cr_1NC, Fe_1Cr_1NC, C-Fe_1NC, and C-Cr_1NC. (c) Impact of nanoparticle shapes on protein corona distribution. Negative-stained TEM images of HApt-functionalized 50NPs and AuNS after protein corona formation and binary images corresponding to the latter. (e) Src and (f) pSrc accumulation in raft domains after different stimulation.

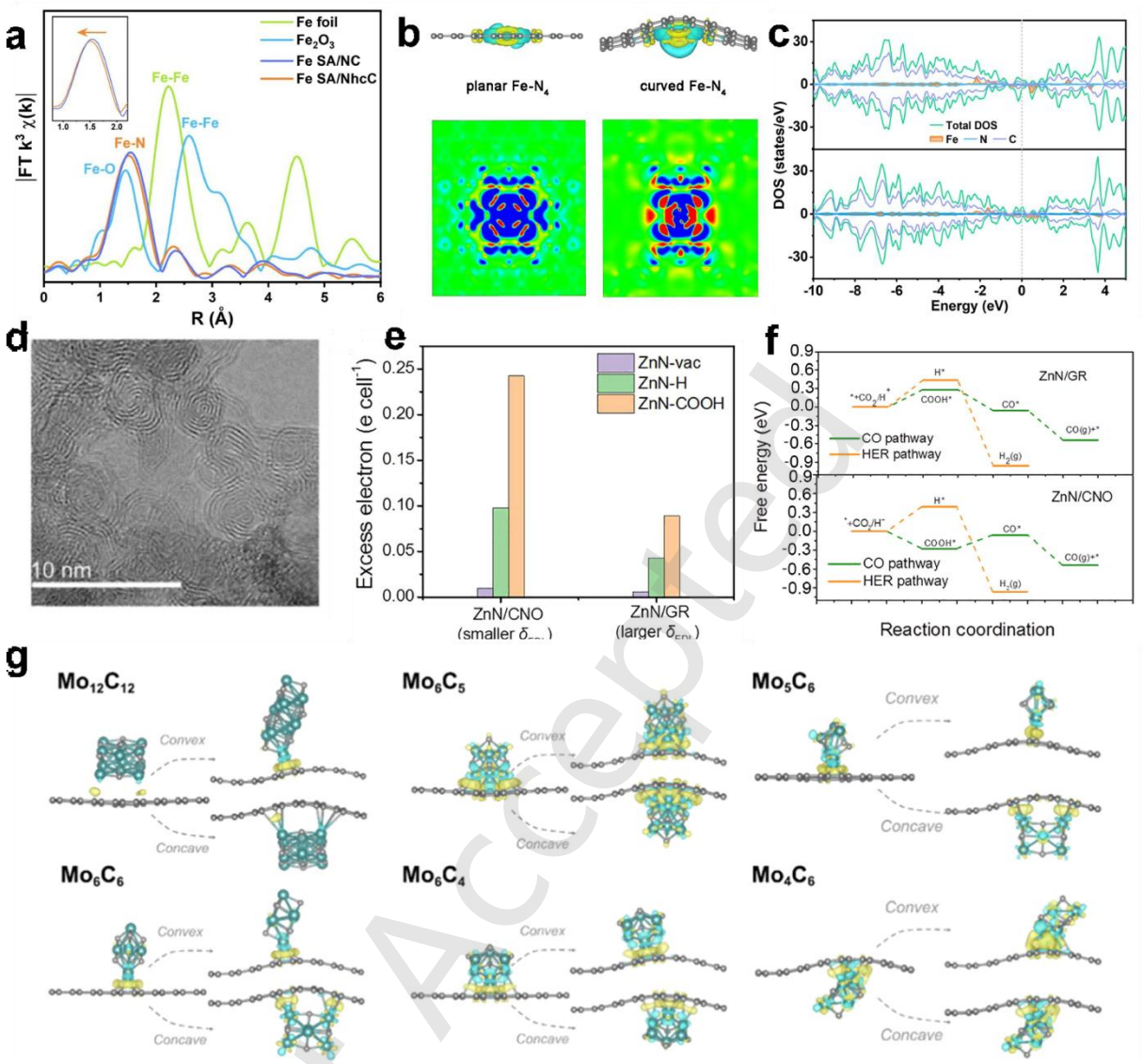

Figure 5. (a) k^3-weighted Fourier-transformed EXAFS spectra of Fe SA/NC, Fe SA/NhcC, Fe foil and Fe_2O_3. (b) analysis of Fe SA/NhcC. Charge density difference and 2D contour plot of the charge density difference of planar Fe-N-C and curved Fe- N-C with a 0.96 strain. (c) Density of states plot for (bottom) planar Fe-N-C and (top) curved Fe-N-C-0.96. (d) HAADF-STEM of ZnN/CNO. (e) The excess electron number in the unit cell for ZnN/CNO and ZnN/GR under URHE = -0.5 V. (f) The reaction free energy diagrams of HER and CO_2RR pathway for ZnN/GR (above) and ZnN/CNO (below) on URHE = -0.48 V. (g) Representative atomic structures of the most stable adsorption of MoC_y NPs on CG.

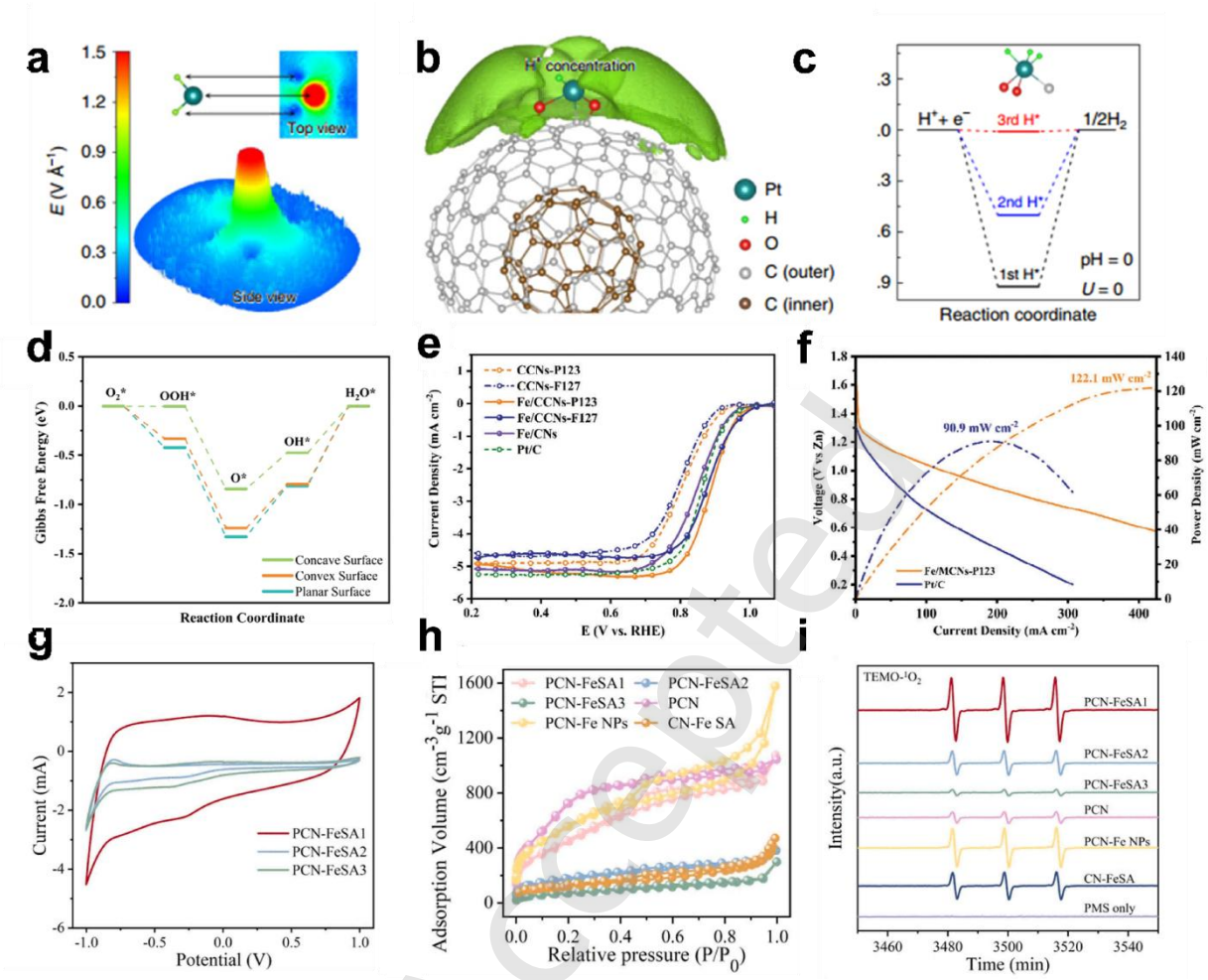

Figure 6. (a)The map of the electric field shows a localized electric field of the H_2Pt_1/OLC system at the tip-like Pt site with an equilibrium potential. (b) Based on the Gouy-Chapman-Stern model, a high concentration of protons (>1.99 mol^{-1}) is distributed around the Pt site (represented by the green shape), which is induced by the local electric field at the Pt site. The grey carbon atoms consist of the outer fullerene-like structure of OLC, whereas the brown carbon atoms represent the inner shell. (c) Calculated free-energy diagram of the HER at the equilibrium potential with pH = 0 and assuming that Pt is the active site. The inset shows the model of H adsorbed on the Pt site, where light green, green, red and grey balls represent, respectively, hydrogen, platinum, oxygen and carbon atoms. (d) Free energy diagrams of intermediates along the reaction coordinate at a potential of 1.23 V. (e) ORR performance catalyzed by Fe/CCNs-P123. LSV curves for various catalysts in 0.1 m KOH. (f) FZAB performances catalyzed by Fe/CCNs-P123. Discharging and power density plots of FZAB. (g) Cyclic voltametric curves of PCN-FeSA1, PCN-FeSA2 and PCN-FeSA3 electrodes. (h) N_2 adsorption-desorption isotherms curves of the catalysts. (i) TEMP based ESR spectra for $^1O_2$ in different system.

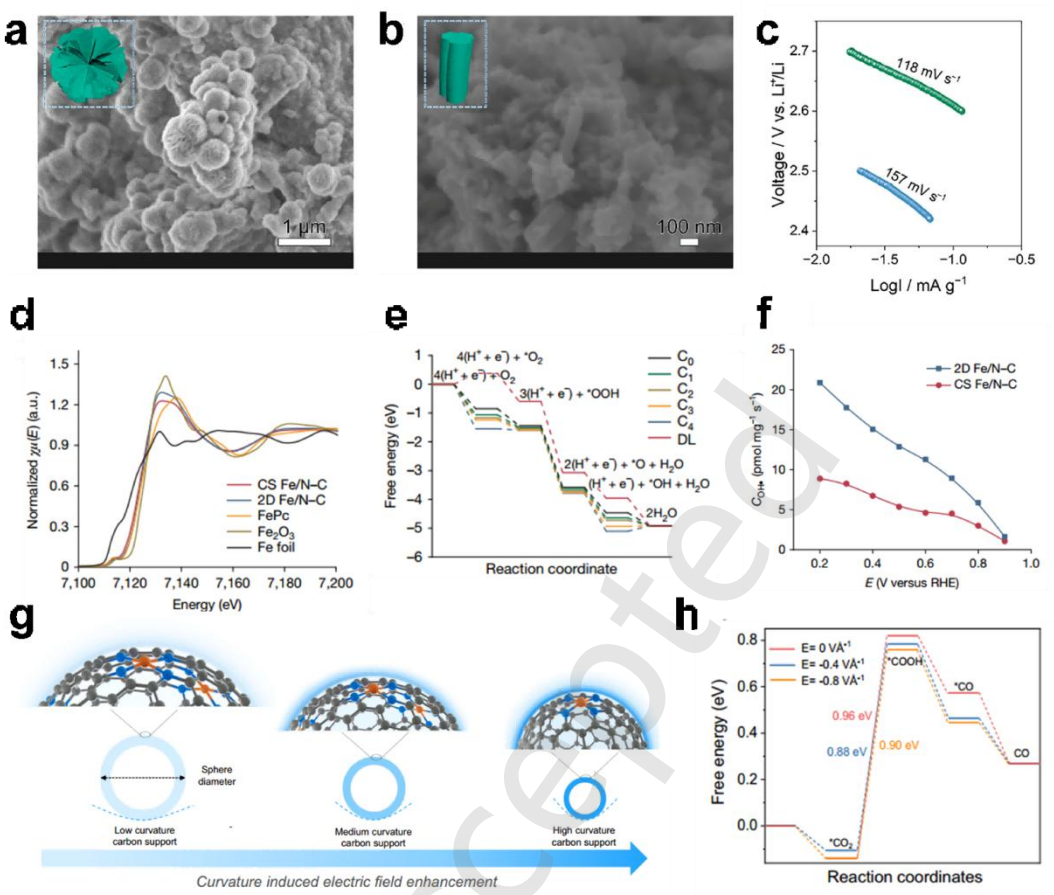

Figure 7. (a, b) SEM images of Ru SACs/rGO and Ru SACs/OCS cathodes. (c) The corresponding Tafel slopes of the Ru SACs/rGO and Ru SACs/OCS. (d) a, Fe K-edge XANES spectra of CS Fe/N-C, 2D Fe/N-C and the reference samples (FePc, Fe_2O_3 and Fe foil). (e) Free energy diagram for ORR. C_0 is the planar model (representing 2D Fe/N-C), C_1 to C_4 are the different curved models and DL is the double layer curved model (representing CS Fe/N-C). (f) Measured hydroxyl radical (*OH) concentration (C) during ORR over 2D Fe/N-C and CS Fe/N-C at different applied potentials. (g) Schematic of our design principle, whereby modulation of the interfacial electric field can be achieved by the carbon support sphere diameter. (h) Reaction pathway Gibbs free energy diagrams.

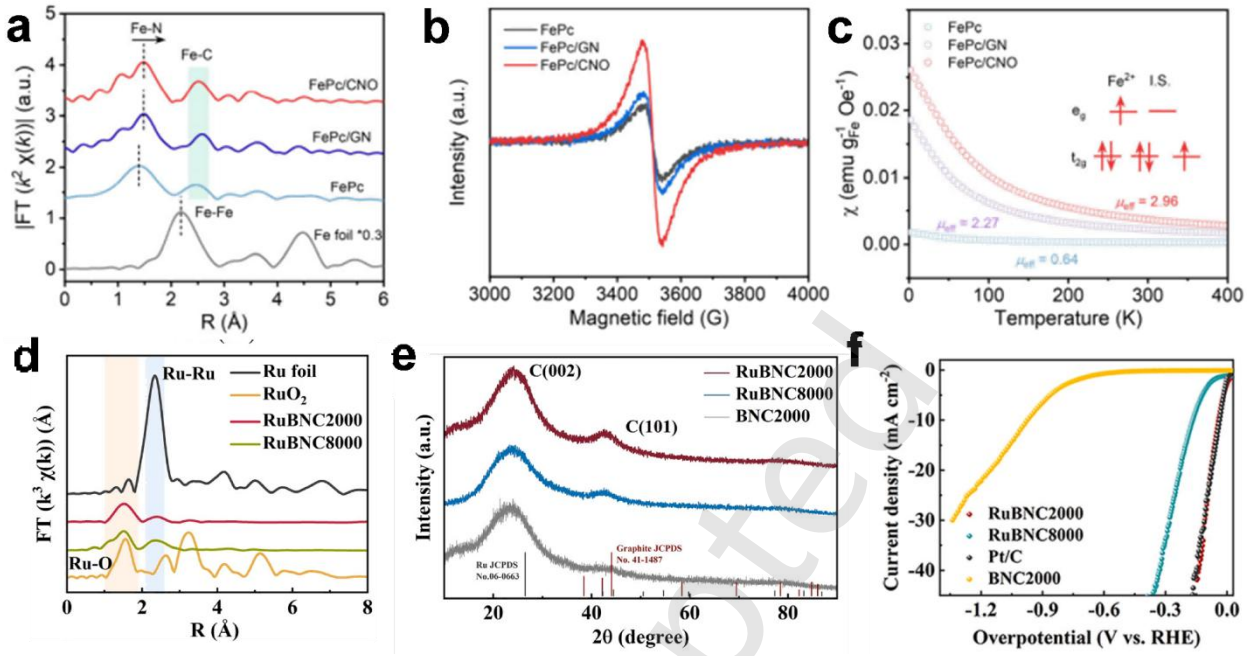

Figure 8. (a) Fourier-transformed Fe K-edge EXAFS spectra. (b) ESR spectra. (c) Temperature-dependent magnetic susceptibility. (d) R-space EXAFS curves of RuBNC2000, RuBNC8000, RuO_2 and Ru foil. (e) XRD patterns. (f) Polarization curves of different samples in 1.0 M KOH.

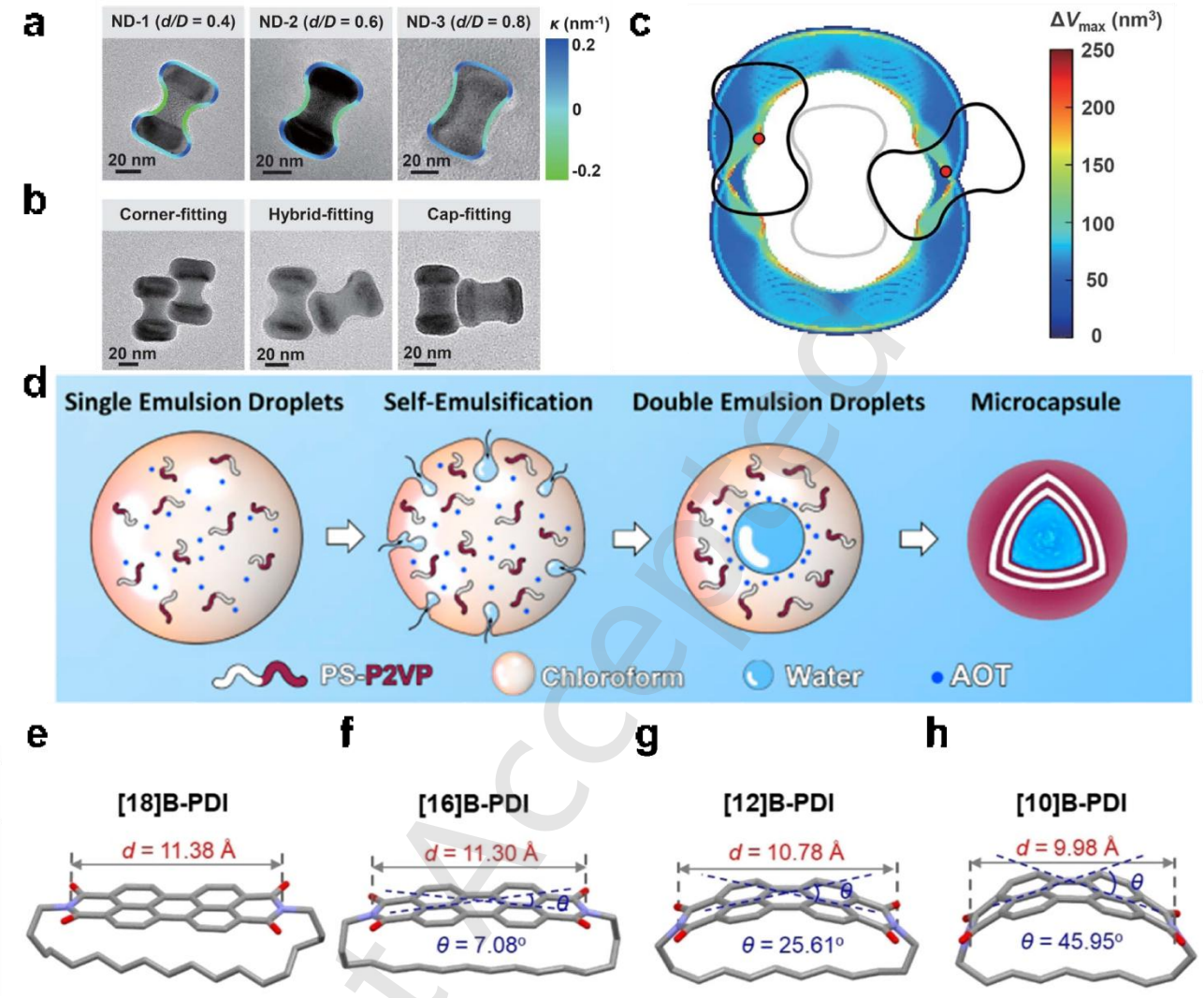

Figure 9. (a)TEM images of NDs with three representative concavities, with their projected contours colorcoded to indicate variations in local curvature (k). (b) TEM images of paired NDs, showing three distinct concave-convex fitting modes between NDs, dictated by their concavity. (c) Calculated ΔV_{max} for ND pairsunder various particle orientations, plotted as a function of relative particle position. The two favored pairing configurations that maximize ΔV_{max} are highlighted with black NDs to indicate the optimal orientations. (d) Illustration showing the formation of PS-b-P2VP PC microcapsules through self-emulsification and emulsion-solvent evaporation. (e-h) Crystal structures and molecular packing arrangements of e) [18]B-PDI, f) [16]B-PDI, g) [12]B-PDI, and h) [10]B-PDI.